Fixed-t subtracted dispersion relations for Compton scattering off the nucleon

D. Drechsel, M. Gorchtein, B. Pasquini, and M. Vanderhaeghen
Institut für Kernphysik, Johannes Gutenberg Universität, D-55099 Mainz, Germany
(Received 9 April 1999; published 20 December 1999)

Fixed-t subtracted dispersion relations are presented for Compton scattering off the nucleon at energies $E_\gamma \leqslant 500$ MeV, as a formalism to extract the nucleon polarizabilities with a minimum of model dependence. The subtracted dispersion integrals are mainly saturated by πN intermediate states in the s channel, $\gamma N \to \pi N \to \gamma N$, and $\pi\pi$ intermediate states in the t channel, $\gamma\gamma \to \pi\pi \to N\bar{N}$. For the subprocess $\gamma\gamma \to \pi\pi$, we construct a unitarized amplitude and find a good description of the available data. We show results for Compton scattering using the subtracted dispersion relations and display the sensitivity on the scalar polarizability difference $\alpha - \beta$ and the backward spin polarizability γ_π, which enter directly as fit parameters in the present formalism. Double polarization observables are shown to have a unique potential for measuring the spin polarizabilities of the nucleon.

PACS number(s): 13.60.Fz, 11.55.Fv, 14.20.Dh, 13.40.−f

I. INTRODUCTION

Compton scattering off the nucleon is determined by six independent helicity amplitudes A_i $(i=1,\dots,6)$, which are functions of two variables, e.g., the Lorentz invariant variables ν (related to the lab energy of the incident photon) and t (related to the momentum transfer to the target). In the limit $\nu \to 0$, the general structure of these amplitudes is governed by low-energy theorems (LET's) based on Lorentz invariance, gauge invariance, and crossing symmetry. These theorems require that (I) the leading term in the expansion in ν is determined by the global properties of the nucleon, i.e., its charge, mass, and anomalous magnetic moment, and (II) the internal structure shows up only at relative order ν^2 and can be parametrized in terms of polarizabilities. In this way there appear six polarizabilities for the nucleon, the familiar electric and magnetic (scalar) polarizabilities α and β, respectively, and four spin (vector) polarizabilities $\gamma_1 - \gamma_4$. These polarizabilities describe the response of the system to an external quasistatic electromagnetic field, and as such they are fundamental structure constants of the composite system.

As a consequence of LET's, the differential cross section for $\nu \to 0$ is given by the (model-independent) Thomson term. In a low-energy expansion, the electric and magnetic polarizabilities then appear as interference between the Thomson term and the subleading terms, i.e., as a contribution of $O(\nu^2)$ in the differential cross section, and α and β can, in principle, be separated by studying the angular distributions. However, it has never been possible to isolate this term and thus to determine the polarizabilities in a model-independent way. The obvious reason is that, for sufficiently small energies, say $\nu \leqslant 40$ MeV, the structure effects are extremely small and hence the statistical errors for the polarizabilities large. At larger energies, however, the higher terms of the expansion, $O(\nu^4)$, become increasingly important. Therefore, a reliable theoretical estimate of these higher terms is of the utmost importance. Moreover, at that order also the spin-dependent polarizabilities come into the game, which has the further consequence that a full determination of the six polarizabilities will require an experimental program with polarized photons and polarized nucleons.

With the advent of high duty-factor electron accelerators and laser backscattering techniques, new precision data have been obtained in the 1990s [1–4] and more experiments are expected in the near future. The presently most accurate values for the proton polarizabilities were derived from the work of MacGibbon *et al.* [4] whose experiments were performed with tagged photons at 70 MeV$\leqslant \nu \leqslant$100 MeV and untagged ones at the higher energies, and analyzed in collaboration with L'vov [5] by means of dispersion relations (in the following denoted by DR's) at constant t. The obtained results were

$$\alpha = (12.1 \pm 0.8 \pm 0.5) \times 10^{-4}\ \text{fm}^3,$$

$$\beta = (2.1 \mp 0.8 \mp 0.5) \times 10^{-4}\ \text{fm}^3. \tag{1}$$

The physics of the $\Delta(1232)$ and higher resonances has been the objective of further recent investigations with tagged photons at Mainz [6,7] and with laser-backscattered photons at Brookhaven [8]. Such data were used to give a first prediction for the so-called backward spin polarizability of the proton, i.e., the particular combination $\gamma_\pi = \gamma_1 + \gamma_2 + 2\gamma_4$ entering the Compton spin-flip amplitude at $\theta = 180°$ [8],

$$\gamma_\pi = -\left[27.1 \pm 2.2\ \ (\text{stat + syst})\ \ {}^{+2.8}_{-2.4}(\text{model})\right] \times 10^{-4}\ \text{fm}^4. \tag{2}$$

In 1991 Bernard *et al.* [9] evaluated the one-loop contributions to the polarizabilities in the framework of relativistic chiral perturbation theory (ChPT), with the result $\alpha = 10 \cdot \beta = 12.1$, (here and in the following, the scalar polarizabilities are given in units of 10^{-4} fm^3 and the spin polarizabilities in units of 10^{-4} fm^4). In order to have a systematic chiral power counting, the calculation was then repeated in heavy baryon ChPT, the expansion parameter being an external momentum or the quark mass. To $O(p^4)$ the result is $\alpha = 10.5 \pm 2.0$ and $\beta = 3.5 \pm 3.6$, the errors being due to four counter terms entering to that order, which were estimated by resonance saturation [10]. One of these counter terms describes the paramagnetic contribution of the $\Delta(1232)$, which is partly canceled by large diamagnetic contributions of pion-nucleon loops. In view of the importance of the Δ resonance, Hemmert, Holstein, and Kambor [11] proposed to include the Δ as a dynamical degree of freedom. This added a further expansion parameter, the difference of the Δ and nucleon masses (''ϵ expansion''). A calculation to $O(\epsilon^3)$ yielded $\alpha=12.2+0+4.2=16.4$ and $\beta=1.2+7.2+0.7=9.1$, the three separate terms referring to contributions of pion-nucleon loops [identical to the predictions of the $O(p^3)$ calculation], Δ-pole terms, and pion-Δ loops [12,13]. These $O(\epsilon^3)$ predictions are clearly at variance with the data, in particular $\alpha+\beta=25.5$ is nearly twice the rather precise value determined from DR's (see below).

The spin polarizabilities have been calculated in both relativistic one-loop ChPT [14] and heavy baryon ChPT [13]. In the latter approach the predictions are $\gamma_0=4.6-2.4-0.2+0=+2.0$, (forward spin polarizability) and $\gamma_\pi=4.6+2.4-0.2-43.5=-36.7$ (backward spin polarizability), the four separate contributions referring to $N\pi$ loops, Δ poles, $\Delta\pi$ loops, and the triangle anomaly, in that order. It is obvious that the anomaly or π^0-pole contribution is by far the most important one to γ_π, and that it would require surprisingly large higher order contributions to increase γ_π to the value of Ref. [8]. Similar conclusions were reached in the framework of DR's. Using the framework of DR's at $t=$const of Ref. [5], Ref. [15] obtained a value of $\gamma_\pi=-34.3$, while L'vov and Nathan [16] worked in the framework of backward DR's and predicted $\gamma_\pi=-39.5\pm2.4$.

As we have stated before, the most quantitative analysis of the experimental data has been provided by DR's. In this way it has been possible to reconstruct the forward non-spin-flip amplitude directly from the total photoabsorption cross section by Baldin's sum rule [17], which yields a rather precise value for the sum of the scalar polarizabilities

$$\begin{aligned}\alpha+\beta&=14.2\pm0.5 \quad (\text{Ref. [18]})\\ &=13.69\pm0.14 \quad (\text{Ref. [19]}).\end{aligned} \tag{3}$$

Similarly, the forward spin polarizability can be evaluated by an integral over the difference of the absorption cross sections in states with helicity 3/2 and 1/2,

$$\begin{aligned}\gamma_0=\gamma_1-\gamma_2-2\gamma_4&=-1.34 \quad (\text{Ref. [20]})\\ &=-0.6 \quad (\text{Ref. [15]}).\end{aligned} \tag{4}$$

While these predictions rely on pion photoproduction multipoles, the helicity cross sections have now been directly determined by scattering photons with circular polarizations on polarized protons [21].

The analysis of Compton scattering at a finite angle requires DR's at $t=\text{const}\leqslant0$, in a range of values between 0 (forward scattering) and the largest negative value of $t=t_{\max}$, determined by the largest scattering angle at the highest photon energy. As mentioned above, the most quantitative and detailed such analysis has been performed by L'vov and collaborators [5,22] in the framework of unsubtracted DR's at $t=$const. Unfortunately, not all of the dispersion integrals converge, as can be inferred from Regge theory. The reason for the divergence of the integrals is essentially given by fixed poles in the t channel, notably the exchange of the neutral pion and of a somewhat fictitious ''σ'' meson with a mass of about 600 MeV and a large width, which models the two-pion continuum with the quantum numbers $I=J=0$. In a more formal view, the dispersion integral is performed along the real axis in the range $-\nu_{\max}\leqslant\nu\leqslant+\nu_{\max}$, with $\nu_{\max}\approx1.5$ GeV, and closed by a semicircle with radius $\nu_{\max}$ in the upper half of the complex ν plane. The contribution of the semicircle is then identified with the asymptotic contribution described by t-channel poles. This introduces unknown vertex functions and the mass of the σ meson, which have to be fitted from the experiment. Moreover, the analysis depends appreciably on the choice of $\nu_{\max}$, and there are substantial contributions of intermediate states beyond the relatively well-known pion-nucleon continuum. These higher states include multipion, η- and ρ-meson production, $\Delta\pi$ loops, and nonresonant s-wave background. The physics behind these effects is certainly worthwhile studying, and there can be no doubt that within the next years we shall learn more about them by detailed coincidence studies of multipion and heavier meson production, but also directly from a careful analysis of Compton scattering at the higher energies [5]. However, the quest for the polarizabilities as fundamental structure constants should not be burdened by too many open questions and phenomenological models.

In view of the problems of unsubtracted DR's, we propose to analyze Compton scattering in the framework of *subtracted* DR's at constant t, with the eventual goal to determine the six polarizabilities with the least possible model dependence. A variant of this method was introduced by Akhmedov and Fil'kov [23], who subtracted at the fixed value $u=M^2$ of the Mandelstam variable u. We choose to subtract the six Compton amplitudes $A_i(\nu,t)$ at the value $\nu=0$, i.e., write subtracted DR's for $A_i(\nu,t)-A_i(0,t)$ at constant t. As we show in the following, these subtracted DR's converge nicely and are quite well saturated essentially by one-pion production. Clearly the price to pay are six new functions $A_i(0,t)$, which have to be determined by another set of DR's, at $\nu=\text{const}=0$ and by use of information obtained from the t-channel reaction $\gamma\gamma\to$ anything. In order to reduce the dependence on the higher intermediate states in the t channel, we subtract again, i.e., write DR's for $A_i(0,t)-A_i(0,0)$, the subtraction constants $A_i(0,0)$ being linear combinations of the six polarizabilities. Since four of these subtraction constants can be calculated from unsubtracted DR's at $t=$const, only two parameters have to be fixed by a fit to low-energy Compton scattering, the combinations $\alpha-\beta$ and γ_π describing the backward non-spin-flip and spin-flip amplitudes, respectively.

In a somewhat similar approach, Holstein and Nathan [24] combined s- and t-channel information to predict the backward scalar polarizability $\alpha-\beta$. Using unsubtracted backward DR's they obtained, from the integration along the lower boundary of the s-channel region, the result $(\alpha-\beta)^s$

$=-6\pm3$, and from the t-channel region a contribution of $(\alpha-\beta)^t\approx 9$. The sum of these two contributions, $\alpha-\beta\approx 3\pm3$, is at variance with the presently accepted experimental (global average) value, $\alpha-\beta=10.0\pm1.5\pm0.9$ [4]. The difficulty to predict this observable is again due to the bad convergence of the integrals in both the s- and the t-channel regions.

In Sec. II we shall give a general introduction to subtracted DR's. This technique is then applied to the cases of DR's at $t=\text{const}$ (s-channel dispersion integral) and DR's at $\nu=0$ (t-channel dispersion integral) in Secs. III and IV, respectively. Our results are compared to the existing low-energy Compton data in Sec. V, and our conclusions are drawn in Sec. VI.

II. FIXED-*t* SUBTRACTED DISPERSION RELATIONS

Assuming invariance under parity, charge conjugation, and time-reversal symmetry, the general amplitude for Compton scattering can be expressed by six independent structure functions $A_i(\nu,t)$, $i=1,\ldots,6$ [5]. These structure functions depend on two Lorentz invariant variables, e.g., ν and t as defined in the following. Denoting the momenta of the initial state photon and proton by q and p, respectively, and with corresponding final-state momenta q' and p', the familiar Mandelstam variables are

$$s=(q+p)^2,\quad t=(q-q')^2,\quad u=(q-p')^2, \tag{5}$$

with the constraint $s+t+u=2M^2$. The variable ν is defined by

$$\nu=\frac{s-u}{4M}=E_\gamma+\frac{t}{4M}, \tag{6}$$

where E_γ is the photon energy in the *lab* frame and M the nucleon mass. The Mandelstam plane is shown in Fig. 1, and the boundaries of the physical and spectral regions are discussed in Appendix A.

The invariant amplitudes A_i are free of kinematical singularities and constraints, and because of the crossing symmetry they satisfy the relation $A_i(\nu,t)=A_i(-\nu,t)$. Assuming further analyticity and an appropriate high-energy behavior, the amplitudes A_i fulfill unsubtracted DR's at fixed t,

$$\mathrm{Re}\,A_i(\nu,t)=A_i^B(\nu,t)+\frac{2}{\pi}\mathcal{P}\int_{\nu_{thr}}^{+\infty}d\nu'\frac{\nu'\,\mathrm{Im}_s A_i(\nu',t)}{\nu'^2-\nu^2}, \tag{7}$$

where A_i^B are the Born (nucleon pole) contributions as in Appendix A of Ref. [5], $\mathrm{Im}_s A_i$ the discontinuities across the s-channel cuts of the Compton process and $\nu_{\mathrm{thr}}=m_\pi+(m_\pi^2+t/2)/(2M)$. However, such unsubtracted DR's require that at high energies ($\nu\to\infty$) the amplitudes $\mathrm{Im}_s A_i(\nu,t)$ drop fast enough so that the integral of Eq. (7) is convergent and the contribution from the semicircle at infinity can be neglected. For real Compton scattering, Regge theory predicts the following high-energy behavior for $\nu\to\infty$ and fixed t [5]:

$$A_{1,2}\sim\nu^{\alpha(t)},$$

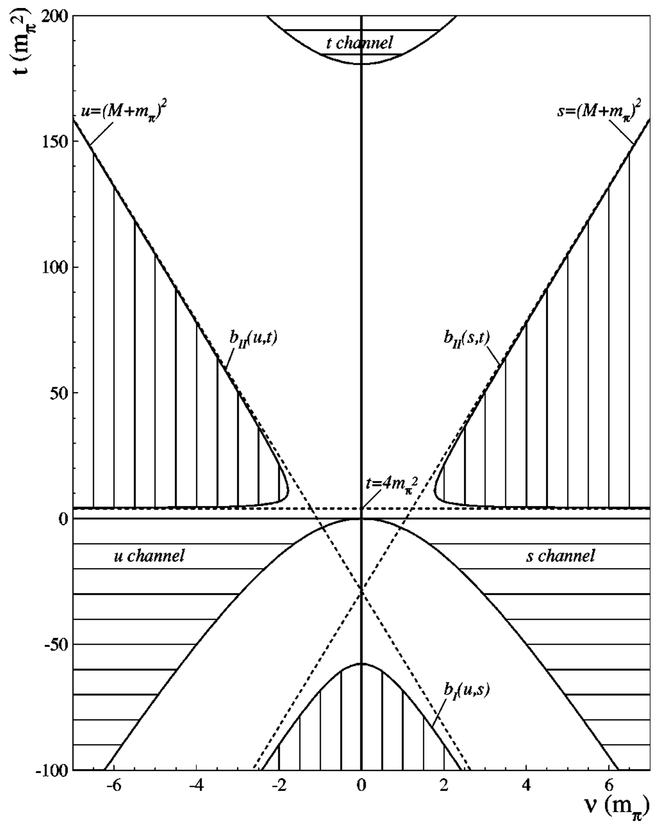

FIG. 1. The Mandelstam plane for Compton scattering. The physical regions are horizontally hatched, whereas the spectral regions are vertically hatched.

$$A_{3,5,6}\sim\nu^{\alpha(t)-2},\quad A_4\sim\nu^{\alpha(t)-3}, \tag{8}$$

where $\alpha(t)\lesssim 1$ is the Regge trajectory. In particular, we note that the Regge trajectory with the highest intercept, i.e., $\alpha(0)\approx 1.08$, corresponds to soft pomeron exchange. Due to the high-energy behavior of Eq. (8), the unsubtracted dispersion integral of Eq. (7) diverges for the amplitudes A_1 and A_2. In order to obtain useful results for these two amplitudes, L'vov *et al.* [5] proposed to close the contour of the integral in Eq. (7) by a semicircle of finite radius $\nu_{\max}$ (instead of the usually assumed infinite radius) in the complex plane, i.e., the real parts of A_1 and A_2 are calculated from the decomposition

$$\mathrm{Re}\,A_i(\nu,t)=A_i^B(\nu,t)+A_i^{\mathrm{int}}(\nu,t)+A_i^{\mathrm{as}}(\nu,t), \tag{9}$$

with A_i^{int} the s-channel integral from pion threshold ν_{thr} to a finite upper limit $\nu_{\max}$, and an ''asymptotic contribution'' A_i^{as} representing the contribution along the finite semicircle of radius $\nu_{\max}$ in the complex plane. In the actual calculations, the s-channel integral is typically evaluated up to a maximum photon energy $E_\gamma=\nu_{\max}(t)-t/(4M)\approx 1.5$ GeV, for which the imaginary part of the amplitudes can be expressed through unitarity by the meson photoproduction amplitudes (mainly 1π and 2π photoproduction) taken from experiment. All contributions from higher energies are then absorbed in the asymptotic term, which is replaced by a finite number of energy-independent poles in the t channel. In particular the asymptotic part of A_1 is parametrized by the exchange of a scalar particle in the t channel, i.e., an effective "σ meson" [5],

$$A_1^{\rm as}(\nu,t) \approx A_1^{\sigma}(t) = \frac{F_{\sigma\gamma\gamma}\, g_{\sigma NN}}{t - m_\sigma^2}, \tag{10}$$

where m_σ is the σ mass, and $g_{\sigma NN}$ and $F_{\sigma\gamma\gamma}$ are the couplings of the σ to nucleons and photons, respectively. In a similar way the asymptotic part of A_2 is described by the π^0 t-channel pole.

This procedure is relatively safe for A_2 because of the dominance of the π^0 pole or triangle anomaly, which is well established both experimentally and on general grounds as the Wess-Zumino-Witten term. However, it introduces a considerable model dependence in the case of A_1. Though σ mesons have been repeatedly reported in the past, their properties were never clearly established. Therefore, this particle should be interpreted as a parametrization of the $I=J=0$ part of the two-pion spectrum, which shows up differently in different experiments and hence has been reported with varying masses and widths.

It is, therefore, the aim of our present contribution to avoid the convergence problem of unsubtracted DR's and the phenomenology necessary to determine the asymptotic contribution. The alternative we shall pursue in the following is to consider DR's at fixed t that are once subtracted at $\nu=0$,

$$\mathrm{Re}\, A_i(\nu,t) = A_i^B(\nu,t) + [A_i(0,t) - A_i^B(0,t)] + \frac{2}{\pi}\nu^2 \mathcal{P}\int_{\nu_{thr}}^{+\infty} d\nu' \frac{\mathrm{Im}_s A_i(\nu',t)}{\nu'(\nu'^2-\nu^2)}. \tag{11}$$

These subtracted DR's should converge for all six invariant amplitudes due to the two additional powers of ν' in the denominator, and they are essentially saturated by the πN intermediate states as will be shown in Sec. III. In other words, the lesser known contributions of two and more pions as well as higher continua are small and may be treated reliably by simple models.

The price to pay for this alternative is the appearance of the subtraction functions $A_i(\nu=0,t)$, which have to be determined at some small (negative) value of t. We do this by setting up the once-subtracted DR, this time in the variable t,

$$\begin{aligned} A_i(0,t) - A_i^B(0,t) = {} & [A_i(0,0) - A_i^B(0,0)] \\ & + [A_i^{t\ \rm pole}(0,t) - A_i^{t\ \rm pole}(0,0)] \\ & + \frac{t}{\pi}\int_{(2m_\pi)^2}^{+\infty} dt' \frac{\mathrm{Im}_t A_i(0,t')}{t'(t'-t)} \\ & - \frac{t}{\pi}\int_{-\infty}^{-2m_\pi^2 - 4Mm_\pi} dt' \frac{\mathrm{Im}_t A_i(0,t')}{t'(t'-t)}, \end{aligned} \tag{12}$$

where $A_i^{t\ \rm pole}(0,t)$ represents the contribution of poles in the t channel, in particular of the π^0 pole in the case of A_2, which is given by

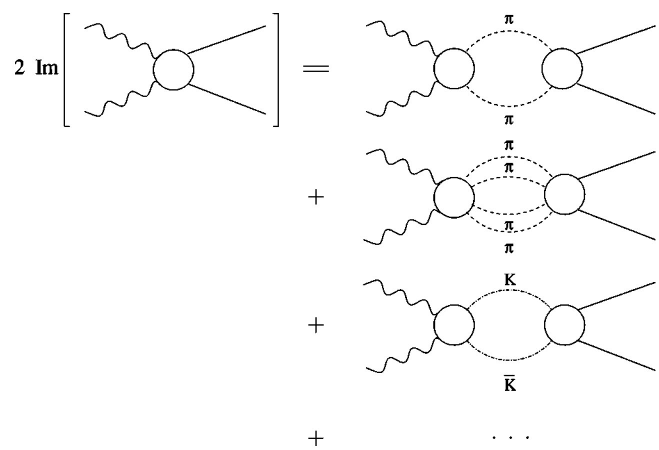

FIG. 2. t-channel unitarity diagrams for Compton scattering.

$$A_2^{\pi^0}(0,t) = \frac{F_{\pi^0\gamma\gamma}\, g_{\pi NN}}{t - m_\pi^2}. \tag{13}$$

The coupling $F_{\pi^0\gamma\gamma}$ is determined through the $\pi^0 \to \gamma\gamma$ decay as

$$\Gamma(\pi^0 \to \gamma\gamma) = \frac{1}{64\pi} m_{\pi^0}^3 F_{\pi^0\gamma\gamma}^2. \tag{14}$$

Using $\Gamma(\pi^0\to\gamma\gamma)=7.74$ eV [25], one obtains $F_{\pi^0\gamma\gamma} = -0.0252\ \mathrm{GeV}^{-1}$, the sign being in accordance with the $\pi^0\gamma\gamma$ coupling in the chiral limit, given by the Wess-Zumino-Witten effective chiral Lagrangian. The πNN coupling is taken from Ref. [26]: $g_{\pi NN}^2/4\pi = 13.72$. This yields then for the product of the couplings in Eq. (13): $F_{\pi^0\gamma\gamma}\, g_{\pi NN} \approx -0.331\ \mathrm{GeV}^{-1}$.

The imaginary part in the integral from $4m_\pi^2 \to +\infty$ in Eq. (12) is saturated by the possible intermediate states for the t-channel process (see Fig. 2), which lead to cuts along the positive t axis. For values of t below the $K\bar{K}$ threshold, the t-channel discontinuity is dominated by $\pi\pi$ intermediate states. The second integral in Eq. (12) extends from $-\infty$ to $-2(m_\pi^2 + 2Mm_\pi) \approx -0.56\ \mathrm{GeV}^2$. The boundary of the su spectral region for $\nu=0$ is given by $-4(m_\pi^2+2Mm_\pi) \approx -1.1\ \mathrm{GeV}^2$ (see Appendix A for a detailed discussion). As we are interested in evaluating Eq. (12) for small (negative) values of t ($|t| \ll |a|$), the integral from $-\infty$ to a will be highly suppressed by the denominator of the subtracted DR's, and will be neglected in this work. Consequently, we shall saturate the subtracted dispersion integrals of Eq. (12) by the contribution of $\pi\pi$ intermediate states, which turns out to be a good approximation for small t. We will show the convergence of the t-channel dispersion integral in Sec. IV and thus verify the quality of the approximation.

The t dependence of the subtraction functions $A_i(0,t)$ is now determined, and only the subtraction constants $A_i(0,0)$ remain to be fixed. We note that the quantities

$$a_i = A_i(0,0) - A_i^B(0,0) \tag{15}$$

are directly related to the polarizabilities. For the spin-independent (scalar) polarizabilities α and β, one finds the two combinations

$$\alpha+\beta=-\frac{1}{2\pi}(a_3+a_6), \tag{16}$$

$$\alpha-\beta=-\frac{1}{2\pi}a_1, \tag{17}$$

related to forward and backward Compton scattering, respectively. Furthermore, the forward combination $\alpha+\beta$ is related to the total absorption spectrum through Baldin's sum rule [17],

$$(\alpha+\beta)_N=\frac{1}{2\pi^2}\int_{\nu_{thr}}^{\infty}d\nu'\frac{\sigma(\gamma N\to X)}{\nu'^2}. \tag{18}$$

The four spin-dependent (vector) polarizabilities γ_1 to γ_4 of Ragusa [27] are defined by

$$\gamma_0\equiv\gamma_1-\gamma_2-2\gamma_4=\frac{1}{2\pi M}a_4, \tag{19}$$

$$\gamma_{13}\equiv\gamma_1+2\gamma_3=-\frac{1}{4\pi M}(a_5+a_6), \tag{20}$$

$$\gamma_{14}\equiv\gamma_1-2\gamma_4=\frac{1}{4\pi M}(2a_4+a_5-a_6), \tag{21}$$

$$\gamma_\pi\equiv\gamma_1+\gamma_2+2\gamma_4=-\frac{1}{2\pi M}(a_2+a_5), \tag{22}$$

where γ_0 and γ_π are the spin polarizabilities in the forward and backward directions, respectively. Since the π^0 pole contributes to A_2 only, the combinations γ_0, γ_{13}, and γ_{14} of Eqs. (19)–(21) are independent of this pole term [15], and only the backward spin polarizability γ_π is affected by the anomaly.

Although all six subtraction constants a_1 to a_6 of Eq. (15) could be used as fit parameters, we shall restrict the fit to the parameters a_1 and a_2, or equivalently to $\alpha-\beta$ and γ_π. The subtraction constants a_4, a_5, and a_6 will be calculated through an unsubtracted sum rule, as derived from Eq. (7),

$$a_{4,5,6}=\frac{2}{\pi}\int_{\nu_{thr}}^{+\infty}d\nu'\frac{\mathrm{Im}_s A_{4,5,6}(\nu',t=0)}{\nu'}. \tag{23}$$

The remaining subtraction constant a_3, which is related to $\alpha+\beta$ through Eq. (16), will be fixed through Baldin's sum rule, Eq. (18), using the value obtained in Ref. [19]: $\alpha+\beta=13.69$.

III. s-CHANNEL DISPERSION INTEGRAL

In this section we describe the calculation of the s-channel contributions, which enter the once-subtracted dispersion integral of Eq. (11) and in the calculation of subtraction constants a_4, a_5, and a_6 through Eq. (23). The imaginary part of the Compton amplitude due to the s-channel cuts is determined from the scattering amplitudes of photoproduction on the nucleon by the unitarity relation

$$2\,\mathrm{Im}_s\,T_{fi}=\sum_X (2\pi)^4\delta^4(P_X-P_i)T^\dagger_{Xf}T_{Xi}, \tag{24}$$

where the sum runs over all possible states that can be formed in the photon-nucleon reaction. Due to the energy denominator $1/\nu'(\nu'^2-\nu^2)$ in the subtracted dispersion integrals, the most important contribution is from the πN intermediate states, while mechanisms involving more pions or heavier mesons in the intermediate states are largely suppressed. In our calculation, we evaluate the πN contribution using the multipole amplitudes from the analysis of Hanstein, Drechsel, and Tiator (HDT) [28] at energies $E_\gamma \leqslant 500$ MeV and at the higher energies we take as input the SAID multipoles (SP98K solution) [29]. The expansion of $\mathrm{Im}_s A_i$ into this set of multipoles is truncated at a maximum angular momentum $j_{\max}=l\pm 1/2=7/2$, with the exception of the lower energy range ($E_\gamma\leqslant 400$ MeV) where we use $j_{\max}=3/2$. The higher partial waves with $j\geqslant j_{\max}+1$ are evaluated analytically in the one-pion exchange (OPE) approximation. The relevant formulas to implement the calculation are reported in Appendix B and C of Ref. [5].

We note that the pion photoproduction multipoles below two-pion threshold were derived in Ref. [28] by use of Watson's theorem, assuming that the pion photoproduction multipoles carry the phases of pion-nucleon scattering. As pointed out by Ref. [30], unitarity also requires to account for the phases of photon-nucleon scattering δ_i^{C}, which is $O(e^2)$ relative to the strong phase. Moreover, consistency requires that isospin-breaking effects be included at the level of the strong scattering amplitudes [30]. Such considerations are of big potential interest, particularly in the threshold region where the pion mass difference becomes important or in studies of the small electric quadrupole strength in the Δ region. However, such effects are beyond the scope of our present work, in particular because only the imaginary part of the amplitudes is needed as input for DR's. As may be seen from Eq. (11) of Ref. [30], this imaginary part is a function of $\cos\delta_i^{\mathrm{C}}$, i.e., corrections are expected to be of order $O(e^4)$.

The multipion intermediate states are approximated by the inelastic decay channels of the πN resonances. In the spirit of Ref. [5] and the more recent work of Ref. [31], we assume that this inelastic contribution follows the helicity structure of the one-pion photoproduction amplitudes. In this approximation, we first calculate the resonant part of the pion photoproduction multipoles using the Breit-Wigner parametrization of Ref. [32], which is then scaled by a suitable factor to include the inelastic decays of the resonances. The resulting contribution to $\mathrm{Im}_s A_i$ is

$$[\mathrm{Im}_s\,A_i]^{(N^*\to\pi\pi N,\,\eta N,\,\dots)}=R[\mathrm{Im}_s\,A_i]^{(N^*\to\pi N)} \tag{25}$$

with the ratio R given by

$$R=\frac{1-B_\pi}{B_\pi}\frac{\overline{\Gamma}_{\rm inel}(W)}{\overline{\Gamma}_\pi(W)}. \tag{26}$$

In Eq. (26), B_π is the single-pion branching ratio of the resonance N^* and $\overline{\Gamma}_\pi(W)$ is the energy-dependent pionic width [32], while the inelastic widths $\overline{\Gamma}_{\rm inel}(W)$ of the decays $N^*\to(\pi\pi N,\eta N,\pi\pi\pi N,\dots)$ are parametrized as in Ref. [5] in order to provide the correct threshold behavior for the resonant two-pion contribution.

The πN channel consistently reproduces the measured photoabsorption cross section in the energy range $E_\gamma \leqslant 500$ MeV, while at the higher energies nonresonant mechanisms should be included to fully describe the multipion channels. In Ref. [5], the nonresonant contribution to the two-pion photoproduction channel was approximately taken into account by calculating the OPE diagram of the $\gamma N\to\pi\Delta$ reaction. The difference between the data and the model for two-pion photoproduction consisting of resonant mechanisms plus the OPE diagram for the nonresonant mechanism, was then fitted in Ref. [5] and attributed to a phenomenological, nonresonant $\gamma N\to\pi\Delta$ s-wave correction term.

A more detailed description of the $\pi\pi N$ channel is clearly worthwhile to be undertaken, especially in view of the new two-pion photoproduction data (both unpolarized and polarized) that will be available from MAMI and JLab (CLAS) in the near future. However, for the extraction of the polarizabilities, the strategy followed in this paper is to minimize sensitivity and hence model uncertainty to these higher channels.

We show in Fig. 3 that in subtracted DR's, the sensitivity to the multipion channels is indeed very small and that subtracted DR's are essentially saturated at $\nu\approx 0.4$ GeV. The importance of the multipion channels is even weaker in the case of the amplitudes A_3–A_6. For unsubtracted DR's, on the other hand, the influence of the multipion channels amounts to about 30% of the amplitude A_2.

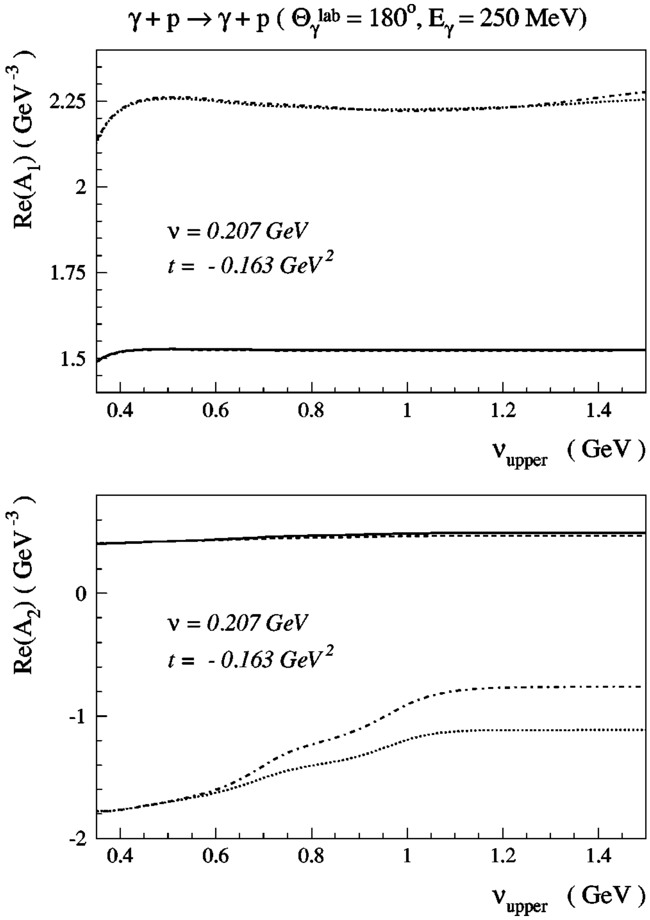

FIG. 3. Convergence of the s-channel integral for the amplitudes A_1 and A_2. Results for the unsubtracted dispersion integral of Eq. (7) for the one-pion channel (dotted lines) and including the two-pion channel (dashed-dotted lines) in comparison with the subtracted dispersion integral of Eq. (11) for the one-pion channel (dashed line) and including the two-pion channel (full lines), as a function of the upper integration limit $\nu_{\rm upper}$.

In Tables I and II, we show our predictions for the dispersion integral of the spin polarizabilities of proton and neutron, respectively. We list the separate contributions of the πN channel, HDT(1π), and the total result, HDT, which includes the inelastic resonance channels. The last column shows the values of the dispersion calculation of Ref. [22],

TABLE I. The contribution of the dispersion integrals to the spin polarizabilities of the proton. The set HDT(1π) is calculated from the one-pion photoproduction multipoles of the HDT analysis [28], while the column HDT gives the total results with the additional contribution of inelastic resonance channels. The entries in the last column are the predictions of the dispersion calculation of Ref. [22].

γ_i − excit.	HDT(1π)	HDT	Ref. [22]
$\gamma_1^{(p)}$	+4.83	+4.33	+3.1
$\gamma_2^{(p)}$	-0.81	-0.74	-0.8
$\gamma_3^{(p)}$	-0.30	-0.02	+0.3
$\gamma_4^{(p)}$	+3.19	+2.93	+2.7
$\gamma_0^{(p)}$	-0.75	-0.80	-1.5
$\gamma_{13}^{(p)}$	+4.23	+4.29	+3.7
$\gamma_{14}^{(p)}$	-1.56	-1.53	-2.3
$\gamma_\pi^{(p)}$	+10.41	+9.46	+7.8

TABLE II. The same as in Table I in the case of the neutron.

γ_i − excit.	HDT(1π)	HDT	Ref. [22]
$\gamma_1^{(n)}$	+7.10	+7.00	+6.3
$\gamma_2^{(n)}$	-0.68	-0.68	-0.9
$\gamma_3^{(n)}$	-1.04	-0.99	-0.7
$\gamma_4^{(n)}$	+3.92	+3.88	+3.8
$\gamma_0^{(n)}$	-0.06	-0.09	-0.4
$\gamma_{13}^{(n)}$	+5.02	+5.02	+4.9
$\gamma_{14}^{(n)}$	-0.74	-0.77	-1.3
$\gamma_\pi^{(n)}$	+14.27	+14.09	+13.0

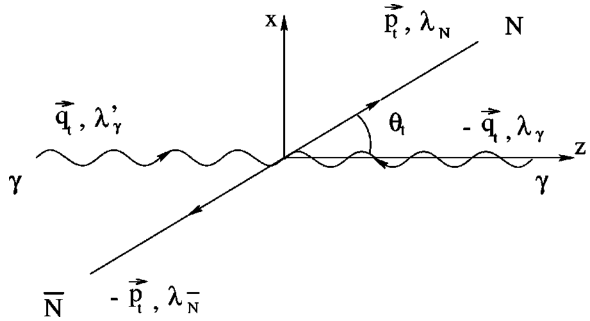

FIG. 4. Kinematics in the c.m. system of the t-channel process $\gamma\gamma \rightarrow N\bar{N}$.

which is based on the one-pion multipoles of SAID-SP97K and the model for double-pion production mentioned above. The small differences between the one-pion multipoles of SAID-SP97K and SAID-SP98K at the higher energies are practically negligible for the spin polarizabilities, while the results are very sensitive to the differences between the HDT and SAID analyses. As discussed in Ref. [33], this fact is mainly due to a different behavior of the E_{0+} partial wave near threshold, giving rise to substantial effects in the case of the forward spin polarizability. While the one-pion contributions from SAID-SP98K are $\gamma_0^p = -1.26$ and $\gamma_0^n = -0.03$, we obtain $\gamma_0^p = -0.75$ and $\gamma_0^n = -0.06$ with the HDT multipoles for $E_\gamma \leqslant 500$ MeV.

IV. t-CHANNEL DISPERSION INTEGRAL

We next evaluate the t-channel dispersion integral in Eq. (12) from $4m_\pi^2$ to ∞. The kinematics of the t-channel reaction $\gamma\gamma \rightarrow N\bar{N}$ is shown in Fig. 4. The subtracted dispersion integral is essentially saturated by the imaginary part of the t-channel amplitude $\gamma\gamma \rightarrow N\bar{N}$ due to $\pi\pi$ intermediate states. To calculate this contribution, we have to construct the amplitudes $\gamma\gamma \rightarrow \pi\pi$ and $\pi\pi \rightarrow N\bar{N}$.

We start with the isospin and helicity structure of the $\gamma\gamma \rightarrow \pi\pi$ amplitude, denoted by F. Because of the Bose symmetry of the $\gamma\gamma$ state, only the even isospin values $I = 0$ and 2 are possible. We can express the charged ($\gamma\gamma \rightarrow \pi^+\pi^-$) and neutral ($\gamma\gamma \rightarrow \pi^0\pi^0$) amplitudes in terms of those with good isospin by

$$F^{(\pi^+\pi^-)} = \sqrt{\frac{2}{3}} F^{I=0} + \sqrt{\frac{1}{3}} F^{I=2} \quad \text{(charged pions)},$$

$$F^{(\pi^0\pi^0)} = -\sqrt{\frac{1}{3}} F^{I=0} + \sqrt{\frac{2}{3}} F^{I=2} \quad \text{(neutral pions)}. \tag{27}$$

The reaction $\gamma\gamma \rightarrow \pi\pi$ has two independent helicity amplitudes $F_{\Lambda_\gamma}(t, \theta_{\pi\pi})$, where $\Lambda_\gamma \equiv \lambda'_\gamma - \lambda_\gamma$, the difference of the final (λ'_γ) and initial (λ_γ) photon helicities, takes on the values 0 or 2, depending upon whether the photons have the same ($\Lambda_\gamma = 0$) or opposite ($\Lambda_\gamma = 2$) helicities. The $\gamma\gamma \rightarrow \pi\pi$ helicity amplitudes depend on t, the c.m. energy

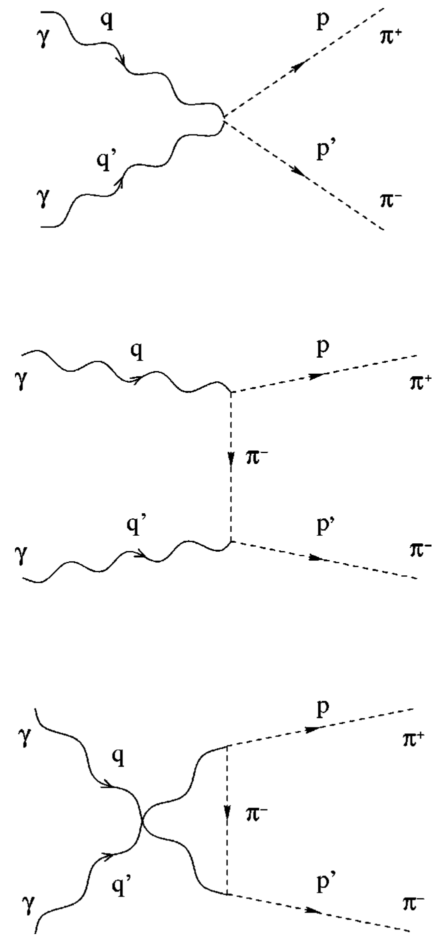

FIG. 5. Born diagrams for the $\gamma\gamma \rightarrow \pi^+\pi^-$ process.

squared, and the pion c.m. scattering angle $\theta_{\pi\pi}$. In terms of the helicity amplitudes F_{Λ_γ}, the $\gamma\gamma \rightarrow \pi\pi$ differential c.m. cross section is given by

$$\left(\frac{d\sigma}{d\cos\theta_{\pi\pi}}\right)_{\text{c.m.}} = \frac{\beta}{64\pi t}\{|F_{\Lambda_\gamma=0}(t, \theta_{\pi\pi})|^2 + |F_{\Lambda_\gamma=2}(t, \theta_{\pi\pi})|^2\} \tag{28}$$

with $\beta = \sqrt{1 - 4m_\pi^2/t}$ being the pion velocity. In Appendix B, we give the partial wave expansion of the $\gamma\gamma \rightarrow \pi\pi$ helicity amplitudes $F^I_{\Lambda_\gamma}(t, \theta_{\pi\pi})$ for a state of isospin I, and thus define the partial wave amplitudes $F^I_{J\Lambda_\gamma}(t)$ [see Eqs. (B6) and (B10)], where J can only take on even values.

To construct the helicity amplitudes F_{Λ_γ} for the process $\gamma\gamma \rightarrow \pi\pi$, we first evaluate the Born graphs as shown in Fig. 5. These graphs only contribute to the charged channel $\gamma\gamma \rightarrow \pi^+\pi^-$. The Born contributions to the helicity amplitudes $F^{(\pi^+\pi^-)}_{\Lambda_\gamma}$ are denoted as B_{Λ_γ} and given by

$$B_{\Lambda_\gamma=0}(t, \theta_{\pi\pi}) = 2e^2 \frac{1-\beta^2}{1-\beta^2\cos^2\theta_{\pi\pi}},$$

$$B_{\Lambda_\gamma=2}(t,\theta_{\pi\pi}) = 2e^2\,\frac{\beta^2\sin^2\theta_{\pi\pi}}{1-\beta^2\cos^2\theta_{\pi\pi}}. \tag{29}$$

The partial wave expansion of the Born terms, $B_{J\Lambda_\gamma}(t)$, is discussed in Appendix B [Eq. (B11)]. As the Born amplitudes are only nonzero for the charged pion channel, the two isospin amplitudes of Eq. (27) are related by

$$B^{I=0}_{J\Lambda_\gamma} = \sqrt{\frac{2}{3}}B_{J\Lambda_\gamma}, \quad B^{I=2}_{J\Lambda_\gamma} = \sqrt{\frac{1}{3}}B_{J\Lambda_\gamma}. \tag{30}$$

We now construct the unitarized amplitudes $F^I_{J\Lambda_\gamma}(t)$, starting from the Born amplitudes $B^I_{J\Lambda_\gamma}(t)$ and following the method outlined in Refs. [34,35]. We first note that the low-energy theorem requires for each partial wave that

$$\frac{F^I_{J\Lambda_\gamma}}{B^I_{J\Lambda_\gamma}} \to 1, \quad \text{as } t\to 0. \tag{31}$$

Next, the invariant amplitude for the process $\gamma\gamma\to\pi\pi$ is assumed to have Mandelstam analyticity. Each partial wave then has a right-hand cut from $t=4m_\pi^2$ to $+\infty$ and a left-hand cut from $t=-\infty$ to 0. Though the Born amplitude is real for all values of t, its partial waves are complex below $t=0$. The partial waves of the full amplitude have no other sources of complexity in this region, and so we can write DR's for the difference of the full and the Born amplitudes,

$$\frac{F^I_{J\Lambda_\gamma}(t)-B^I_{J\Lambda_\gamma}(t)}{t(t-4m_\pi^2)^{J/2}} = \frac{1}{\pi}\int_{4m_\pi^2}^{\infty} dt'\,\frac{\mathrm{Im}\,F^I_{J\Lambda_\gamma}(t')}{t'(t'-4m_\pi^2)^{J/2}(t'-t)} \tag{32}$$

with an additional factor of $[t(t-4m_\pi^2)^{J/2}]^{-1}$ providing the right asymptotics for the convergence of the integral. The next step is to evaluate the imaginary part of the amplitude in Eq. (32). To do this, we exploit the unitarity condition

$$\mathrm{Im}\,F^I_{J\Lambda_\gamma}(\gamma\gamma\to\pi\pi) = \sum_n \rho_n F^{I*}_{J\Lambda_\gamma}(\gamma\gamma\to n)\mathcal{I}^I_J(n\to\pi\pi), \tag{33}$$

where ρ_n are the appropriate kinematical and isospin factors for the intermediate channels n, and $\mathcal{I}(n\to\pi\pi)$ is a hadronic amplitude. Below the next inelastic threshold, it follows from unitarity that the phase $\phi_J^{I(\gamma\gamma\to\pi\pi)}$ of each partial wave $F^I_{J\Lambda_\gamma}$ is equal to the phase $\delta^{IJ}_{\pi\pi}$ of the corresponding $\pi\pi\to\pi\pi$ partial wave,

$$\mathrm{Im}\,F^I_{J\Lambda_\gamma}(\gamma\gamma\to\pi\pi) = \rho_{\pi\pi}F^{I*}_{J\Lambda_\gamma}(\gamma\gamma\to\pi\pi)\mathcal{I}^I_J(\pi\pi\to\pi\pi)$$

$$\Downarrow$$

$$\phi_J^{I(\gamma\gamma\to\pi\pi)}(t) = \delta^{IJ}_{\pi\pi}(t). \tag{34}$$

This fact can be incorporated into the Omnès function, which is constructed to have the phase of the $\pi\pi$ scattering amplitude above $\pi\pi$ threshold, and to be real otherwise,

$$\Omega^I_J(t) = \exp\left[\frac{t}{\pi}\int_{4m_\pi^2}^{\infty} dt'\,\frac{\delta^{IJ}_{\pi\pi}(t')}{t'(t'-t-i\varepsilon)}\right]. \tag{35}$$

The function $F^I_{J\Lambda_\gamma}(\Omega^I_J)^{-1}(t)$ is by construction real above the $\pi\pi$ threshold, but complex below the threshold due to the complexity of the Born partial waves $B^I_{J\Lambda_\gamma}$. Hence, we can write a dispersion relation for $[F^I_{J\Lambda_\gamma}-B^I_{J\Lambda_\gamma}]\times(\Omega^I_J)^{-1}(t)/t(t-4m_\pi^2)^{J/2}$,

$$F^I_{J\Lambda_\gamma}(t) = \Omega^I_J(t)\Bigg\{B^I_{J\Lambda_\gamma}(t)\mathrm{Re}[(\Omega^I_J)^{-1}(t)] - \frac{t(t-4m_\pi^2)^{J/2}}{\pi}\int_{4m_\pi^2}^{\infty} dt'\,\frac{B^I_{J\Lambda_\gamma}(t')\mathrm{Im}[(\Omega^I_J)^{-1}(t')]}{t'(t'-4m_\pi^2)^{J/2}(t'-t)}\Bigg\}. \tag{36}$$

For $t>4m_\pi^2$, this integral is understood to be a principal value integral, which we implement by subtracting the integrand at $t'=t$. In this way we obtain a regular integral, which can be performed without numerical problems,

$$F^I_{J\Lambda_\gamma}(t) = \Omega^I_J(t)\Bigg\{B^I_{J\Lambda_\gamma}(t)\left[\mathrm{Re}[(\Omega^I_J)^{-1}(t)] + \mathrm{Im}[(\Omega^I_J)^{-1}(t)]\frac{1}{\pi}\ln\left(\frac{t}{4m_\pi^2}-1\right)\right] - \frac{t(t-4m_\pi^2)^{J/2}}{\pi}\int_{4m_\pi^2}^{\infty}\frac{dt'}{t'(t'-t)}\left(\frac{B^I_{J\Lambda_\gamma}(t')\mathrm{Im}[(\Omega^I_J)^{-1}(t')]}{(t'-4m_\pi^2)^{J/2}} - \frac{B^I_{J\Lambda_\gamma}(t)\mathrm{Im}[(\Omega^I_J)^{-1}(t)]}{(t-4m_\pi^2)^{J/2}}\right)\Bigg\}. \tag{37}$$

In our formalism, the $s(J=0)$ and $d(J=2)$ waves are unitarized. For the s- and d-wave $\pi\pi$ phaseshifts, we use the solutions that were determined in Ref. [36]. For the higher partial waves, the corresponding $\pi\pi$ phaseshifts are rather small and not known with good precision. Therefore, we will approximate all higher partial waves $(J\geq 4)$ by their Born contribution. The full amplitudes for the charged and neutral channels can then be cast into the forms

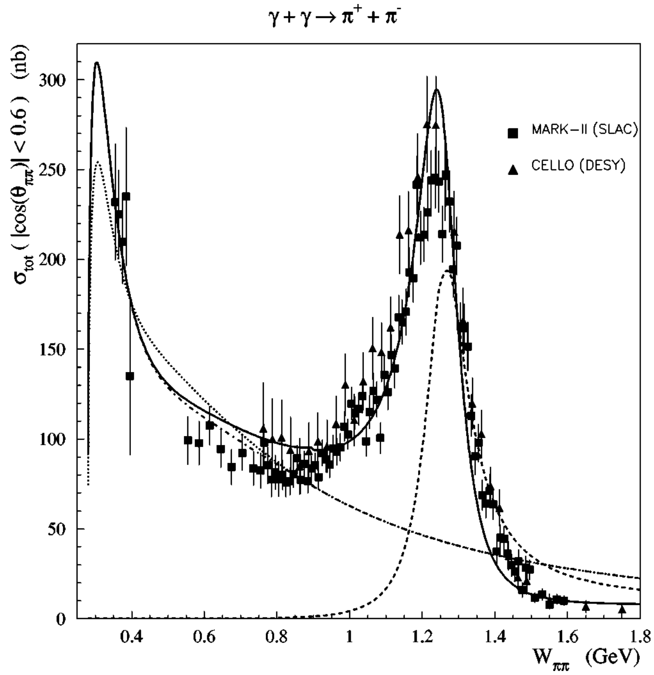

FIG. 6. Total cross section for the $\gamma\gamma\to\pi^+\pi^-$ process as function of the c.m. energy: Born terms (dotted line), Born amplitude with unitarized s-wave (dashed-dotted line), $f_2(1270)$ resonance contribution (dashed line), and total amplitude (full line).

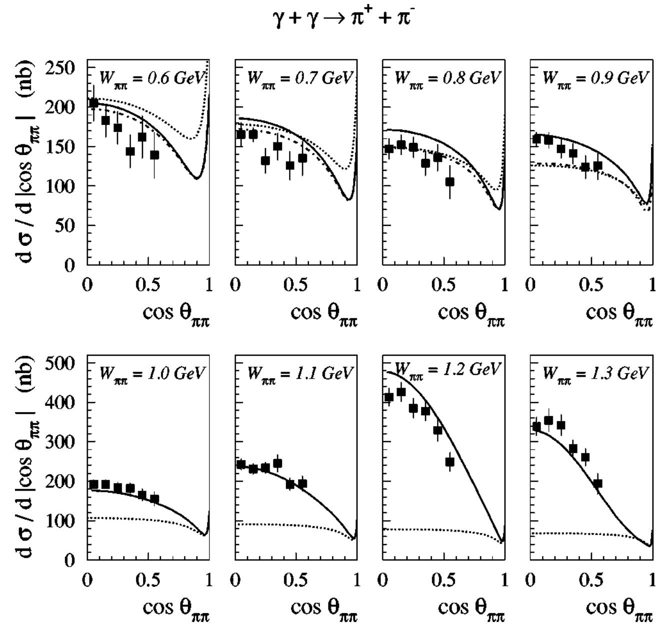

FIG. 7. Differential cross section at various c.m. energies for the $\gamma\gamma\to\pi^+\pi^-$ process: Born terms (dotted line), Born amplitude with unitarized s-wave (dashed-dotted line, only shown at the four lower energies), and total amplitude including the $f_2(1270)$ resonance contribution (full line).

$$F_{\Lambda_\gamma}^{(\pi^+\pi^-)}(t,\theta_{\pi\pi})=B_{\Lambda_\gamma}(t,\theta_{\pi\pi})+\sum_{J=0,2}\sqrt{2J+1}\sqrt{\frac{(J-\Lambda_\gamma)!}{(J+\Lambda_\gamma)!}}\times\left[\sqrt{\frac{2}{3}}F_{J\Lambda_\gamma}^{I=0}(t)+\sqrt{\frac{1}{3}}F_{J\Lambda_\gamma}^{I=2}(t)-B_{J\Lambda_\gamma}(t)\right]P_J^{\Lambda_\gamma}(\cos\theta_{\pi\pi}), \tag{38}$$

$$F_{\Lambda_\gamma}^{(\pi^0\pi^0)}(t,\theta_{\pi\pi})=\sum_{J=0,2}\sqrt{2J+1}\sqrt{\frac{(J-\Lambda_\gamma)!}{(J+\Lambda_\gamma)!}}\left[-\sqrt{\frac{1}{3}}F_{J\Lambda_\gamma}^{I=0}(t)+\sqrt{\frac{2}{3}}F_{J\Lambda_\gamma}^{I=2}(t)\right]P_J^{\Lambda_\gamma}(\cos\theta_{\pi\pi}). \tag{39}$$

These expressions hold to good precision up to the $K\bar{K}$ threshold ($\approx 1\ \mathrm{GeV}^2$), because the four-pion intermediate states couple only weakly and give only small inelasticities in the $\pi\pi$ phaseshifts.

In Figs. 6 and 7, we show our results for the total and differential $\gamma\gamma\to\pi^+\pi^-$ cross sections and a comparison to the existing data. In the threshold region, the charged pion cross sections are clearly dominated by the Born graphs of Fig. 5 because of the vicinity of the pion pole in the t channel of the $\gamma\gamma\to\pi^+\pi^-$ process. However, the results for the unitarized calculation show that s-wave rescattering is not negligible but leads to a considerable enhancement at energies just above threshold. Besides the low-energy structure, which is driven by the Born terms, the $\gamma\gamma\to\pi\pi$ process has a prominent resonance structure at energies corresponding to excitation of the isoscalar $f_2(1270)$ resonance, with mass m_{f_2} = 1275 MeV and width $\Gamma_{f_2}=185.5$ MeV [25]. The f_2 resonance shows up in the partial wave $F_{J=2\Lambda_\gamma=2}$ as outlined in Appendix C. Therefore, the most efficient way to unitarize this particular partial wave is to make a Breit-Wigner ansatz for the f_2 excitation, which is described in Appendix C. The Breit-Wigner ansatz for the f_2 contribution to the partial wave $F_{J=2\Lambda_\gamma=2}$ depends upon the couplings $f_2\pi\pi$ and $f_2\gamma\gamma$. The coupling $f_2\pi\pi$ is known from the decay $f_2\to\pi\pi$ and is taken from Ref. [25]. The coupling $f_2\gamma\gamma$ is then fitted to the $\gamma\gamma\to\pi\pi$ cross section at the f_2 resonance position, and is consistent with the value quoted in Ref. [25]. The resulting amplitude, consisting of unitarized s-wave, f_2 excitation and Born terms for all other partial waves (with $J\geqslant 4$) is seen from Figs. 6 and 7 to give a rather good description of the $\gamma\gamma\to\pi^+\pi^-$ data up to $W_{\pi\pi}\simeq 1.8$ GeV. Only in the region $W_{\pi\pi}\approx 0.7$–0.8 GeV, does our description slightly overestimate the data.

Having constructed the $\gamma\gamma\to\pi\pi$ amplitudes, we next need the $\pi\pi\to N\bar{N}$ amplitudes in order to estimate the contribution of the $\pi\pi$ states to the t-channel dispersion integral for Compton scattering. As we only kept s and d waves for $\gamma\gamma\to\pi\pi$, we will only need the s and d waves ($J=0,2$) for $\pi\pi\to N\bar{N}$. For each partial wave J, there are two independent $\pi\pi\to N\bar{N}$ helicity amplitudes $f_\pm^J(t)$, depending on whether the nucleon and antinucleon have the same $[f_+^J(t)]$ or opposite $[f_-^J(t)]$ helicities. We refer the reader to Appendix B [Eqs. (B7) and (B9)] for details. In this work, we take the s and d waves from the work of Höhler and collaborators [37], in which the lowest $\pi\pi\to N\bar{N}$ partial wave amplitudes were constructed from a partial wave solution of pion-nucleon scattering, by use of the $\pi\pi$ phaseshifts of Ref. [36], which we also used to construct the $\gamma\gamma\to\pi\pi$ amplitudes. In Ref. [37], the $\pi\pi\to N\bar{N}$ amplitudes are given for t values up to $t\approx 40\cdot m_\pi^2\approx 0.78\ \mathrm{GeV}^2$, which will serve well for our purpose since the subtracted t-channel dispersion integrals have converged much below this value as shown in the following.

Finally, we can now combine the $\gamma\gamma\to\pi\pi$ and $\pi\pi\to N\bar{N}$ amplitudes to construct the discontinuities of the Compton amplitudes across the t-channel cut. In Appendix B, we show in detail how the Compton invariant amplitudes $A_1,\ldots,A_6$ are expressed by the t-channel ($\gamma\gamma\to N\bar{N}$) helicity amplitudes. Through unitarity we then express the imaginary parts of these t-channel ($\gamma\gamma\to N\bar{N}$) helicity amplitudes in terms of the $\gamma\gamma\to\pi\pi$ and $\pi\pi\to N\bar{N}$ amplitudes. We finally express the discontinuities $\mathrm{Im}_t A_i$ of the invariant amplitudes A_i ($i=1,\ldots,6$) in terms of the corresponding $\gamma\gamma\to\pi\pi$ and $\pi\pi\to N\bar{N}$ partial wave amplitudes [see Eq. (B12)]. As we restrict ourselves to s- and d-wave intermediate states in the actual calculations, we give the expressions at $\nu=0$, including s and d waves only, that are needed for the subtracted t-channel dispersion integral of Eq. (12):

$$
\begin{aligned}
\mathrm{Im}_t A_1(\nu=0,t)^{2\pi}
&= -\sqrt{\frac{t/4-m_\pi^2}{t}}\frac{1}{t(M^2-t/4)}F_{0\Lambda_\gamma=0}(t)f_+^{0*}(t)\\
&\quad -\left(\frac{t/4-m_\pi^2}{t}\right)^{3/2}\frac{\sqrt{5}}{2}F_{2\Lambda_\gamma=0}(t)f_+^{2*}(t),\\
\mathrm{Im}_t A_2(\nu=0,t)^{2\pi}&=0,\\
\mathrm{Im}_t A_3(\nu=0,t)^{2\pi}
&= -\left(\frac{t/4-m_\pi^2}{t}\right)^{3/2}\frac{M^2}{(M^2-t/4)}\frac{\sqrt{5}}{2}F_{2\Lambda_\gamma=2}(t)\\
&\quad \times\left\{\sqrt{\frac{3}{2}}f_+^{2*}(t)-Mf_-^{2*}(t)\right\},\\
\mathrm{Im}_t A_4(\nu=0,t)^{2\pi}&=0,\\
\mathrm{Im}_t A_5(\nu=0,t)^{2\pi}
&= -\left(\frac{t/4-m_\pi^2}{t}\right)^{3/2}M\sqrt{\frac{15}{2}}F_{2\Lambda_\gamma=0}(t)f_-^{2*}(t),\\
\mathrm{Im}_t A_6(\nu=0,t)^{2\pi}&=-\left(\frac{t/4-m_\pi^2}{t}\right)^{3/2}M\frac{\sqrt{5}}{2}F_{2\Lambda_\gamma=2}(t)f_-^{2*}(t).
\end{aligned}
\tag{40}
$$

The reader should note that the s-wave $\pi\pi$ intermediate state only contributes to the amplitude A_1. It is the t dependence of this $I=J=0$ $\pi\pi$ state in the t channel that is approximated in Ref. [5] and parametrized by a σ pole. The d-wave $\pi\pi$ intermediate state gives rise to imaginary parts for the amplitudes A_1,A_3,A_5, and A_6. The amplitude A_2 (at $\nu=0$) corresponds to the t-channel exchange of an object with the quantum numbers of one pion [e.g., π^0 pole in Eq. (13)], therefore two-pion intermediate states do not contribute to A_2. The imaginary part of A_4 receives only contributions from $\pi\pi$ intermediate states with $J\geqslant 4$ [see Eq. (B12)] and, therefore, is zero in our description, as we keep only s and d waves.

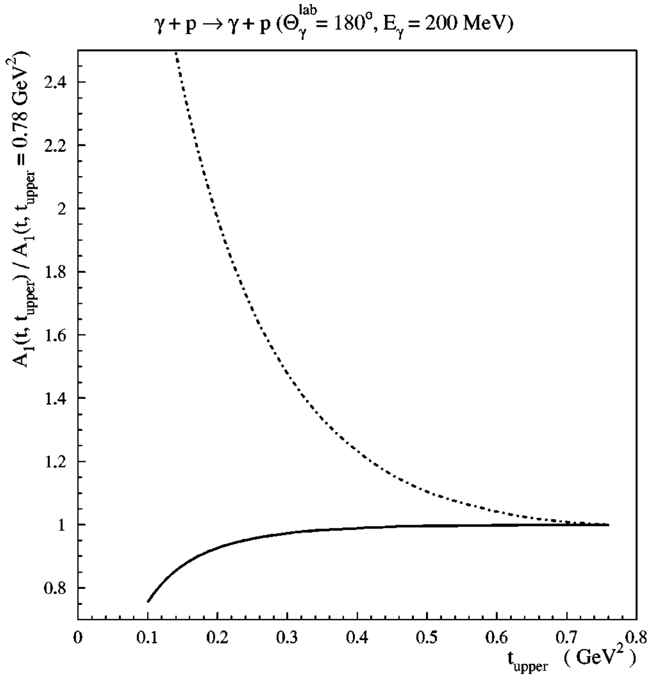

FIG. 8. Convergence of the t-channel integral for the amplitude A_1. The results for the unsubtracted (dashed curve) and the subtracted (full curve) t-channel dispersion integrals are shown as function of the upper integration limit t_{upper}. Both results are normalized to their respective values at $t_{\mathrm{upper}}=0.78\ \mathrm{GeV}^2$.

In Fig. 8 we show the convergence of the t-channel integral from $4m_\pi^2$ to ∞ in the subtracted DR's of Eq. (12). We do so by calculating the dispersion integral as function of the upper integration limit t_{upper} and by showing the ratio to the integral for $t_{\mathrm{upper}}=0.78\ \mathrm{GeV}^2$. The latter value corresponds to the highest t value for which the $\pi\pi\to N\bar{N}$ amplitudes are given in Ref. [37]. One clearly sees from Fig. 8 that the unsubtracted t-channel DR shows only a slow convergence, whereas the subtracted t-channel DR has already reached its final value, within the percent level, at a t value as low as 0.4 GeV^2. Although the cross section $\gamma\gamma\to\pi\pi$ shows appreciable strength above $t>0.78\ \mathrm{GeV}^2$ (see Fig. 6), its contribution to the Compton amplitudes is negligibly small due to the subtraction in the t-channel integral. By estimating the $\pi\pi\to N\bar{N}$ d-wave amplitudes in Born approximation, we checked that the influence of the $f_2(1270)$ resonance on the Compton observables shown in the following section does not exceed 1% and usually is even smaller.

V. RESULTS AND DISCUSSION

In this section we shall present our results for Compton scattering off the nucleon in the dispersion formalism pre-

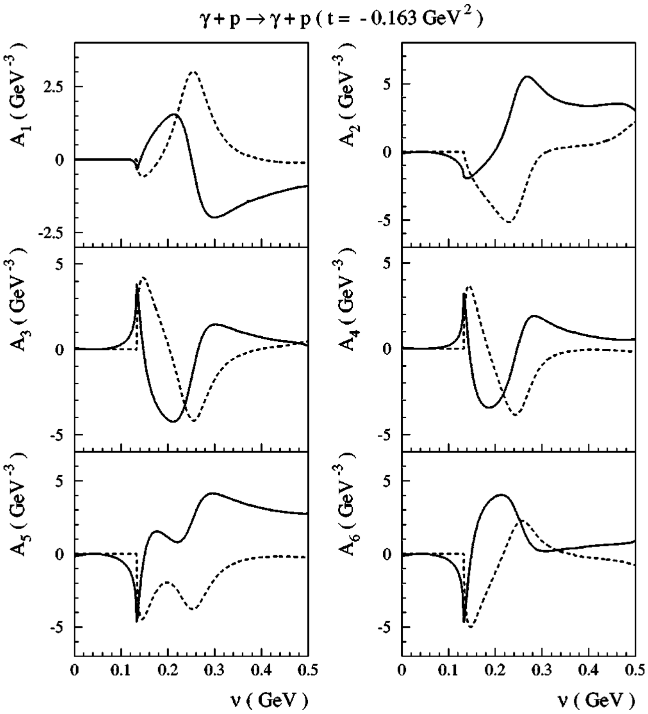

FIG. 9. Real part (full lines) of the subtracted s-channel integral [see Eq. (11)] and imaginary part [see Eq. (24)] of the invariant Compton amplitudes $A_1, \ldots, A_6$ as function of ν at fixed $t = -0.163\ \mathrm{GeV}^2$.

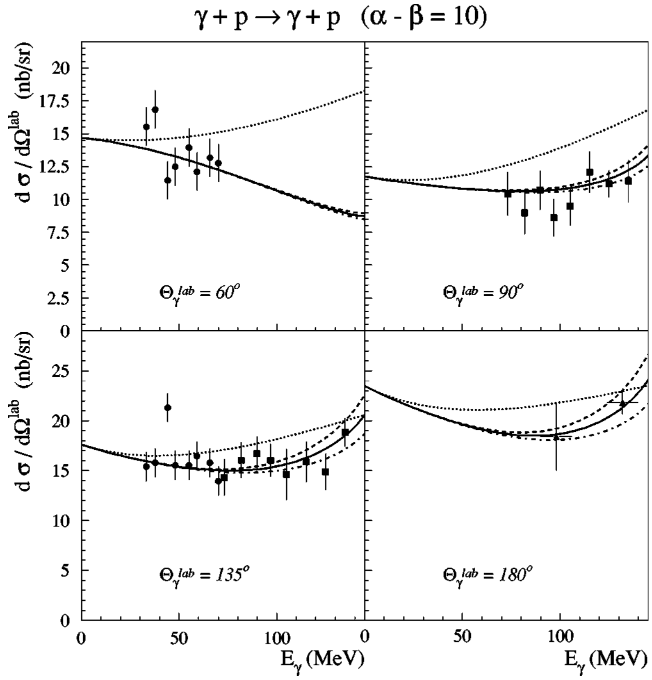

FIG. 10. Differential cross section for Compton scattering off the proton as function of the lab photon energy E_γ and at four scattering angles $\Theta_\gamma^{\mathrm{lab}}$. The Born result is given by the dotted lines. The total results of the subtracted dispersion formalism are shown for fixed $\alpha-\beta=10$ and different values of γ_π: $\gamma_\pi=-37$ (dashed-dotted lines), $\gamma_\pi=-32$ (full lines), and $\gamma_\pi=-27$ (dashed lines). The data are from Ref. [1] (circles), Ref. [2] (triangles), and Ref. [4] (squares).

sented above. The real and imaginary parts of the six Compton amplitudes are displayed in Fig. 9. Note that for the real part, we only show the subtracted s-channel integral of Eq. (11). As can be seen from Fig. 9, these amplitudes show strong oscillations due to interference effects between different pion photoproduction multipoles, in particular between threshold pion production (E_{0+}) and Δ excitation (M_{1+}).

In Figs. 10 and 11 we show our predictions in the subtracted dispersion relation formalism and compare them with the available Compton data on the proton below pion threshold. These data were used in Ref. [4] to determine the scalar polarizabilities α and β through a global fit, with the results given in Eq. (1). In the analysis of Ref. [4], the unsubtracted dispersion relation formalism was used and the asymptotic contributions [Eq. (9)] to the invariant Compton amplitudes A_1 and A_2 were parametrized. In particular, A_2^{as} was described by the π^0 pole, which yields the value $\gamma_\pi \simeq -45$. The free parameter entering in A_1^{as} was related to $\alpha-\beta$, for which the fit obtained the value $\alpha-\beta\simeq 10$. Keeping $\alpha-\beta$ fixed at that value, we demonstrate in Fig. 10 that the sensitivity to γ_π is not at all negligible, especially at the backward angles and the higher energies. We investigate this further in Fig. 11, where we show our results for different $\alpha-\beta$ and for a fixed value of $\gamma_\pi=-37$, which is consistent with the heavy baryon ChPT prediction [13] and close to the value obtained in Ref. [16] in a backward dispersion relation formalism. For that value of γ_π, a better description of the data (in particular at the backward angles) seems to be possible by using a smaller value for $\alpha-\beta$ than determined in Ref. [4].

As one moves to energies above the pion threshold, the Compton cross section rises rapidly because of the unitarity coupling to the much stronger pion photoproduction channel. Therefore this higher energy region is usually considered less "pure" to extract polarizabilities because the procedure would require a rather precise knowledge of pion photoproduction. With the new pion photoproduction data on the proton that have become available in recent years, the energy region above pion threshold could, however, serve as a valuable complement to determine the polarizabilities, provided one can minimize the model uncertainties in the dispersion formalism. In this work, we use the most recent information on the pion photoproduction channel by taking the HDT [28] multipoles at energies $E_\gamma \leqslant 500$ MeV and the SAID-SP98K solution [29] at higher energies. As previously shown in Fig. 3, the subtracted DR's are practically saturated by the one-pion channel for photon energies through the Δ region, which minimizes the uncertainty due to the modeling of the two-pion photoproduction channels. In Fig. 12 we display the high sensitivity of the Compton cross sections to γ_π in the lower part of the Δ region. This sensitivity was exploited in Ref. [8] within the context of an unsubtracted dispersion relation formalism, and the value $\gamma_\pi \simeq -27$ was extracted from the LEGS 97 data, which are shown at the higher energies in Fig. 12. Our results for the subtracted DR are obtained in Fig. 12 at fixed $\alpha-\beta=10$ and for γ_π varying between -27 and -37. We found that the lower energy data ($E_\gamma=149$ and 182 MeV) can be easily described by the larger values of γ_π if $\alpha-\beta$ decreases to some value below

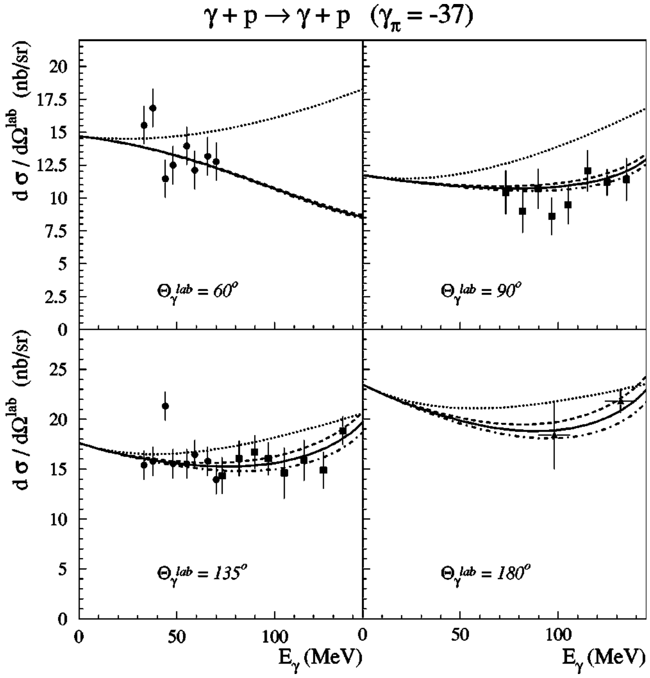

FIG. 11. Differential cross section for Compton scattering off the proton as a function of the lab photon energy E_γ and at four scattering angles $\Theta_\gamma^{\rm lab}$ as in Fig. 10. The Born result is given by the dotted lines. The total results of the subtracted dispersion formalism are presented for fixed $\gamma_\pi = -37$ and different values of $\alpha - \beta$: $\alpha - \beta = 10$ (dashed-dotted lines), $\alpha - \beta = 8$ (full lines), and $\alpha - \beta = 6$ (dashed lines). Data as described in Fig. 10.

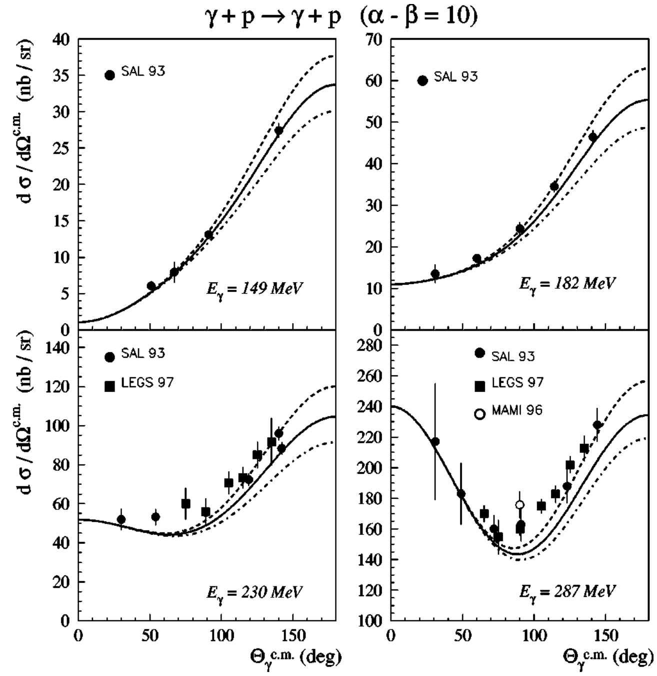

FIG. 12. Differential cross section for Compton scattering off the proton as function of the c.m. photon angle for different lab energies. The total results of the subtracted DR formalism are presented for fixed $\alpha - \beta = 10$ and different values of γ_π: $\gamma_\pi = -37$ (dashed-dotted lines), $\gamma_\pi = -32$ (full lines), and $\gamma_\pi = -27$ (dashed lines). The data are from Ref. [3] (solid circles), Refs. [6,7] (open circles), and Ref. [8] (squares).

10. On the other hand, the higher energy data ($E_\gamma = 230$ and 287 MeV) seem to favor a smaller value of γ_π, and so far we confirm the conclusion reached in Ref. [8]. However, as will be discussed next, our calculation underpredicts the data around 90° in the lower part of the Δ region.

In the same energy region, there also exist both differential cross section and photon asymmetry data obtained at LEGS [38] by use of the laser backscattering technique. In Fig. 13 we compare our predictions with these data. One finds that at both energies ($E_\gamma = 265$ MeV and 323 MeV) our subtracted dispersion relation formalism provides a good description of the asymmetries, which however show little sensitivity on γ_π, but underestimates the absolute values of the cross sections. In particular close to the resonance position at $E_\gamma = 323$ MeV, our formalism does not allow us to find any reasonable combination of γ_π and $\alpha - \beta$ to describe these data. Therefore, within the present formalism, the actual data situation at these higher energies does not seem to be very conclusive with regard to a value of γ_π. Since the uncertainties due to two-pion and heavier meson photoproduction in the s channel as well as t-channel contributions above the $f_2(1270)$ resonance are expected to be less than 1%, the only possibility to describe the $E_\gamma = 323$ MeV LEGS data would be an increase of the HDT M_{1+} multipole by about 2.5% (see the dotted lines in Fig. 13). Indeed such a fit was obtained by Tonnison *et al.* [8] by use of the LEGS pion photoproduction multipole set of Ref. [38] for photon energies between 200 and 350 MeV and the SAID-SM95 multipole solution [29] outside this interval. However, the more recent SAID-SP98K solution is in very close agreement with the HDT multipoles in the Δ region and hence the prediction with the new SAID solution also falls below the data at 323 MeV in Fig. 13.

In view of the somewhat inconclusive situation, we are waiting for the new MAMI data for Compton scattering on the proton in and above the Δ-resonance region and over a wide angular range that have been reported preliminarly [39]. These new data will be most valuable to check the consistency of pion photoproduction and Compton scattering results obtained at LEGS, MAMI, and other facilities.

Finally, in Fig. 14 we show that double polarization observables will be ultimately necessary to extract the spin polarizabilities. In particular, an experiment with a circularly polarized photon and a polarized proton target displays quite some sensitivity on the backward spin polarizability γ_π, especially at energies between threshold and the Δ resonance. Such a measurement would be more selective to γ_π due to a much lesser sensitivity to $\alpha - \beta$ (see Fig. 14).

VI. CONCLUSIONS

We have presented a formalism of fixed-t subtracted dispersion relations for Compton scattering off the nucleon at energies $E_\gamma \leqslant 500$ MeV. Due to the subtraction, the s-channel dispersion integrals converge very fast and are practically saturated by the πN intermediate states, which are described by the recent pion photoproduction multipoles of HDT. In this way we minimize the uncertainties from

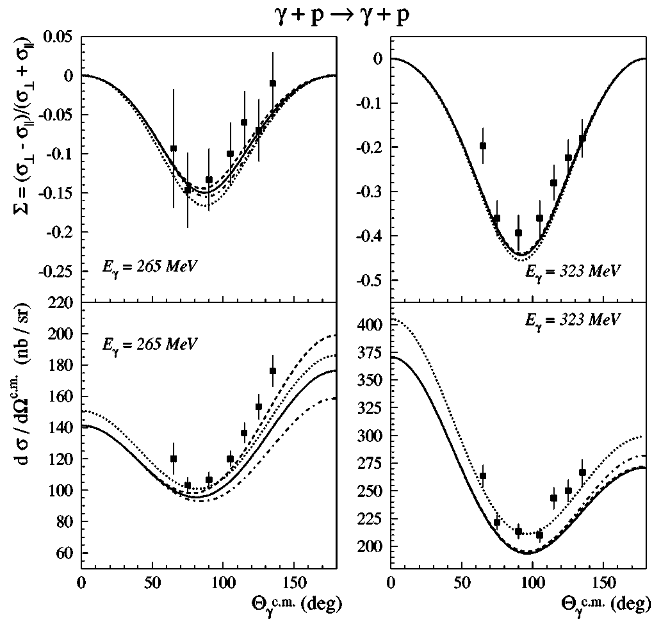

FIG. 13. Photon asymmetries (upper panels) and differential cross sections (lower panels) for Compton scattering off the proton in the Δ resonance region. The total results of the subtracted DR formalism are shown for fixed $\alpha-\beta=10$ and different values of γ_π: $\gamma_\pi=-37$ (dashed-dotted lines), $\gamma_\pi=-32$ (full lines), and $\gamma_\pi=-27$ (dashed lines). We also show the result for $\alpha-\beta=10$ and $\gamma_\pi=-32$ when increasing the HDT M_{1+} multipole by 2.5% (dotted lines). The data are from LEGS [38].

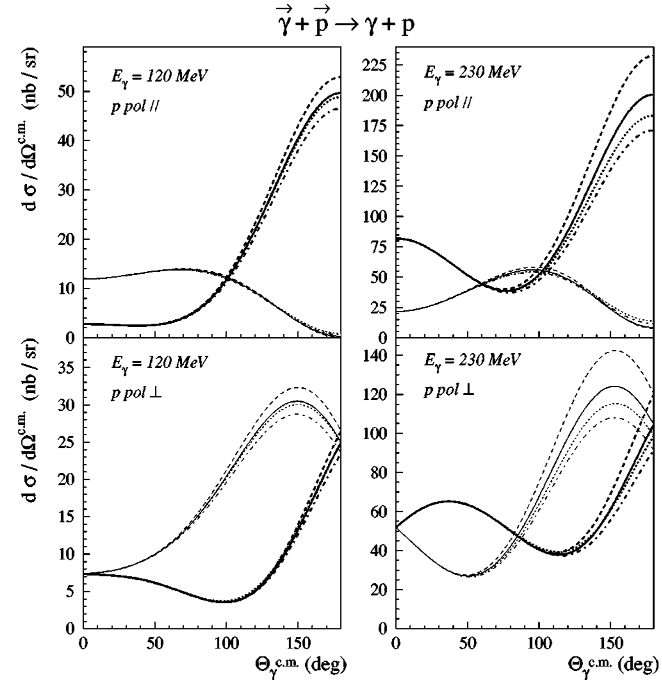

FIG. 14. Double polarization differential cross sections for Compton scattering off the proton, with circularly polarized photon and target proton polarized along the photon direction (upper panels) or perpendicular to the photon direction and in the plane (lower panels). The thick (thin) lines correspond to a proton polarization along the positive (negative) direction, respectively. The results of the dispersion calculation are for $\alpha-\beta=10$ and different values for γ_π: $\gamma_\pi=-32$ (full lines), $\gamma_\pi=-27$ (dashed lines), and $\gamma_\pi=-37$ (dashed-dotted lines). We also show the result for $\alpha-\beta=8$ and $\gamma_\pi=-37$ (dotted lines).

multipion and heavier meson intermediate states.

To calculate the dependence of the subtraction functions on momentum transfer t, we include the experimental information on the t-channel process through $\pi\pi$ intermediate states as $\gamma\gamma\to\pi\pi\to N\bar{N}$. We construct a unitarized amplitude for the $\gamma\gamma\to\pi\pi$ subprocess and find a good description of the available data. This information is then combined with the $\pi\pi\to N\bar{N}$ amplitudes determined from dispersion theory by analytical continuation of πN scattering. In this way, we also avoid the uncertainties in Compton scattering associated with the two-pion continuum in the t channel, which is usually modeled through the exchange of a somewhat fictitious σ meson. Altogether we estimate that the uncertainties in the s- and t-channel integrals, due to unknown high-energy contributions, should be less than 1%. As a consequence our formalism provides a direct cross check between Compton scattering and one-pion photoproduction. In particular, it will become possible to study the consistency between the Compton scattering and pion photoproduction data sets at LEGS and MAMI. At present, the existing pion photoproduction data unfortunately differ by about 10% in the Δ region. We repeat that in Compton scattering near the Δ resonance, the leading M_{1+} multipole of pion photoproduction will enter to the fourth power, and thus has to be known very precisely in order to describe the cross section over the full angular range.

Since the polarizabilities enter as subtraction constants, the subtracted dispersion relation formalism can be used to extract the nucleon polarizabilities from the data with a minimum of model dependence. However, the existing data are not sufficient to determine $\alpha-\beta$ and γ_π independently, especially because of the mentioned normalization problem regarding the M_{1+} multipole. This situation could improve with the analysis of new Compton data, both below pion threshold and in the Δ region, in particular if the normalization problem can be resolved.

A full study of the spin (or vector) polarizabilities will, however, require double polarization experiments. As we have shown, the scattering of polarized photons on polarized protons is very sensitive to γ_π, in particular in the backward hemisphere and at energies between threshold and the Δ-resonance region. In addition, possible normalization problems can be avoided by measuring appropriate asymmetries. Therefore, such polarization experiments hold the promise of disentangling scalar and vector polarizabilities of the nucleon and to quantify the nucleon-spin response in an external electromagnetic field.

ACKNOWLEDGMENTS

The authors are grateful to G. Krein, A. L'vov, and members of the A2 Collaboration, in particular J. Ahrens, V. Olmos de Léon, and F. Wissmann, for useful discussions. This work was supported by the Deutsche Forschungsgemeinschaft (SFB 443) and in part by the Marie Curie TMR program (Contract No. ERBFMBICT972758).

APPENDIX A: THE MANDELSTAM PLANE—PHYSICAL AND SPECTRAL REGIONS FOR COMPTON SCATTERING

The kinematics of Compton scattering, $\gamma(q)N(p) \to \gamma(q')N(p')$, can be described in terms of the familiar Mandelstam variables,

$$s=(q+p)^2, \quad t=(q-q')^2, \quad u=(q-p')^2 \tag{A1}$$

with the constraint

$$s+t+u=2M^2. \tag{A2}$$

Furthermore, we introduce the coordinate ν perpendicular to t,

$$\nu=\frac{s-u}{4M}=E_\gamma+\frac{t}{4M}. \tag{A3}$$

In these equations, E_γ is the photon energy in the lab frame and M is the nucleon mass.

The boundaries of the physical regions in the s, u, and t channels are determined by the zeros of the Kibble function Φ,

$$\Phi(s,t,u)=t(us-M^4)=0. \tag{A4}$$

The three physical regions are shown by the horizontally hatched areas in Fig. 1. The vertically hatched areas are the regions of nonvanishing double spectral functions. These spectral regions are those regions in the Mandelstam plane where two of the three variables s,t, and u take on values that correspond with a physical (i.e., on-shell) intermediate state. The boundaries of these regions follow from unitarity. As discussed in Ref. [37], it is sufficient to consider two-particle intermediate states in all channels. Since these boundaries depend only on the masses, they are the same for all six amplitudes A_i. In the Mandelstam diagram of Fig. 1 they are symmetric to the line $\nu=0$ due to crossing symmetry. For the spectral function ρ_{su} we obtain the boundary

$$\begin{aligned} b_I(u,s)&=b_I(s,u)\\ &=[s-(M+m_\pi)^2][u-(M+m_\pi)^2]\\ &\quad-(m_\pi^2+2Mm_\pi)^2\\ &=0, \end{aligned} \tag{A5}$$

and for the spectral function ρ_{st} we find

$$\begin{aligned} b_{II}(s,t)=&(t-4m_\pi^2)[s-(M+m_\pi)^2][s-(M-m_\pi)^2]\\ &-8m_\pi^4(s+M^2-m_\pi^2/2)=0. \end{aligned} \tag{A6}$$

The boundary of the spectral function ρ_{ut} follows from crossing symmetry. We also note that these boundaries are obtained for the isovector photon, which couples to a $\pi^+\pi^-$ pair. The corresponding boundaries for the isoscalar photon are inside the boundaries of Eqs. (A5) and (A6), because it couples to three pions.

APPENDIX B: *t*-CHANNEL HELICITY AMPLITUDES FOR COMPTON SCATTERING

The t-channel helicity amplitudes for Compton scattering can be expressed in the orthogonal basis of Prange [40] in terms of the invariants $T_1, \ldots, T_6$. In the c.m. system of the t-channel process $\gamma\gamma\to N\bar{N}$ (see Fig. 4 for the kinematics), we choose the photon momentum $\vec{q}_t$ (helicity λ'_γ) to point in the z direction and the nucleon momentum $\vec{p}\,'=\vec{p}_t$ in the xz plane at an angle θ_t with respect to the z axis (the antinucleon momentum is then given by $-\vec{p}=-\vec{p}_t$). In this frame, the t-channel helicity amplitudes can be cast into the form

$$\begin{aligned} T^t_{\lambda_N\lambda_{\bar{N}},\lambda'_\gamma\lambda_\gamma}(\nu,t)=&(-1)^{1/2-\lambda_{\bar{N}}}\bar{u}(\vec{p}_t,\lambda_N)\\ &\times\Big\{-\frac{1}{2}\lambda'_\gamma\lambda_\gamma(T_1+|\vec{q}_t|\gamma^3T_2)\\ &-\frac{1}{2}(T_3+|\vec{q}_t|\gamma^3T_4)-\frac{1}{2}(\lambda'_\gamma+\lambda_\gamma)\gamma_5T_5\\ &-\frac{1}{2}(\lambda'_\gamma-\lambda_\gamma)\gamma_5|\vec{q}_t|\gamma^3T_6\Big\}\\ &\times v(-\vec{p}_t,\lambda_{\bar{N}}), \end{aligned} \tag{B1}$$

which behave under parity transformation as

$$T^t_{\lambda_N\lambda_{\bar{N}},\lambda'_\gamma\lambda_\gamma}(\nu,t)=(-1)^{\Lambda_N-\Lambda_\gamma}T^t_{-\lambda_N-\lambda_{\bar{N}},-\lambda'_\gamma-\lambda_\gamma}(\nu,t), \tag{B2}$$

with the helicity differences Λ_γ and Λ_N given by $\Lambda_\gamma=\lambda'_\gamma-\lambda_\gamma$ (with $\Lambda_\gamma=0$ or 2) and $\Lambda_N=\lambda_N-\lambda_{\bar{N}}$ (with $\Lambda_N=0$ or 1), respectively.

However, the invariant amplitudes $T_i(i=1,\ldots,6)$ of Prange have kinematical constraints and behave differently under $s\leftrightarrow u$ crossing. While T_1, T_3, T_5, and T_6 are even functions of ν, T_2 and T_4 are odd functions (note that $\nu\to-\nu$ is equivalent to $s\leftrightarrow u$). Therefore, L'vov [5] used a new set of invariant amplitudes $A_i(i=1,\ldots,6)$, which are all even functions of ν and are at the same time free of kinematical singularities. The relation between the amplitudes T_i and A_i can be found in Appendix A of Ref. [5], together with the definition of a similar set of amplitudes due to Bardeen and Tung [41]. We express the invariant amplitudes $A_i(\nu,t)$ $(i=1,\ldots,6)$ in terms of the t-channel helicity amplitudes $T^t_{\lambda_N\lambda_{\bar{N}},\lambda'_\gamma\lambda_\gamma}(\nu,t)$ of Eq. (B1), for which we have found the expressions

$$A_1=\frac{1}{t\sqrt{t-4M^2}}\left\{[T^t_{1/2\;1/2,11}+T^t_{1/2\;1/2,-1-1}]-2\nu\frac{\sqrt{t}}{\sqrt{su-M^4}}T^t_{1/2-1/2,11}\right\},$$

$$A_2=\frac{1}{t\sqrt{t}}\left\{-[T^t_{1/2\;1/2,11}-T^t_{1/2\;1/2,-1-1}]-\frac{2\nu\sqrt{t-4M^2}}{\sqrt{su-M^4}}T^t_{1/2-1/2,11}\right\},$$

$$A_3=\frac{M^2}{su-M^4}\,\frac{1}{\sqrt{t-4M^2}}\left\{2T^t_{1/2\;1/2,1-1}+\frac{\sqrt{su-M^4}}{\nu\sqrt{t}}[T^t_{1/2-1/2,1-1}+T^t_{1/2-1/2,-11}]\right\},$$

$$A_4=\frac{M^2}{su-M^4}\,\frac{1}{\sqrt{su-M^4}}\left\{M[-T^t_{1/2-1/2,1-1}+T^t_{1/2-1/2,-11}]+\frac{\sqrt{t}\sqrt{t-4M^2}}{4\nu}[T^t_{1/2-1/2,1-1}+T^t_{1/2-1/2,-11}]\right\},$$

$$A_5=\frac{\sqrt{t-4M^2}}{4\nu\sqrt{t}\sqrt{su-M^4}}\{-2T^t_{1/2-1/2,11}\},$$

$$A_6=\frac{\sqrt{t-4M^2}}{4\nu\sqrt{t}\sqrt{su-M^4}}\{[T^t_{1/2-1/2,1-1}+T^t_{1/2-1/2,-11}]\}. \tag{B3}$$

In the subtracted DR's of Eq. (12), the t-channel integral runs along the line $\nu=0$. Therefore, we have to determine the imaginary parts $\mathrm{Im}_t A_i(\nu=0,t)$ of the invariant amplitudes of Eq. (B3). We start by decomposing of the t-channel helicity amplitudes for $\gamma\gamma\to N\bar{N}$ into a partial wave series,

$$T^t_{\lambda_N\lambda_{\bar{N}},\lambda'_\gamma\lambda_\gamma}(\nu,t)=\sum_J\frac{2J+1}{2}T^J_{\lambda_N\lambda_{\bar{N}},\lambda'_\gamma\lambda_\gamma}(t)\,d^J_{\Lambda_N\Lambda_\gamma}(\theta_t), \tag{B4}$$

where $d^J_{\Lambda_N\Lambda_\gamma}$ are Wigner d functions and θ_t is the scattering angle in the t channel, which is related to the invariants ν and t by $\cos\theta_t=4M\nu/\sqrt{t}\sqrt{t-4M^2}$. It is obvious from this equation that $\nu=0$ corresponds to 90° scattering for the t-channel process. As explained in Sec. IV, we calculate the imaginary parts of the t-channel helicity amplitudes $T^t_{\lambda_N\lambda_{\bar{N}},\lambda'_\gamma\lambda_\gamma}(\nu,t)$ through the unitarity equation by inserting $\pi\pi$ intermediate states, which should give the dominant contribution below $K\bar{K}$ threshold,

$$2\,\mathrm{Im}\,T_{\gamma\gamma\to N\bar{N}}=\frac{1}{(4\pi)^2}\,\frac{|\vec{p}_\pi|}{\sqrt{t}}\int d\Omega_\pi[T_{\gamma\gamma\to\pi\pi}][T_{\pi\pi\to N\bar{N}}]^*. \tag{B5}$$

Combining the partial wave expansion for $\gamma\gamma\to\pi\pi$,

$$T^{\gamma\gamma\to\pi\pi}_{\Lambda_\gamma}(t,\theta_{\pi\pi})=\sum_{J\ \mathrm{even}}\frac{2J+1}{2}T^{J(\gamma\gamma\to\pi\pi)}_{\Lambda_\gamma}(t)\times\sqrt{\frac{(J-\Lambda_\gamma)!}{(J+\Lambda_\gamma)!}}P^{\Lambda_\gamma}_J(\cos\theta_{\pi\pi}), \tag{B6}$$

and the partial wave expansion for $\pi\pi\to N\bar{N}$,

$$T^{\pi\pi\to N\bar{N}}_{\Lambda_N}(t,\Theta)=\sum_J\frac{2J+1}{2}T^{J(\pi\pi\to N\bar{N})}_{\Lambda_N}(t)\times\sqrt{\frac{(J-\Lambda_N)!}{(J+\Lambda_N)!}}P^{\Lambda_N}_J(\cos\Theta). \tag{B7}$$

We can now construct the imaginary parts of the Compton t-channel partial waves,

$$2\,\mathrm{Im}\,T^{J(\gamma\gamma\to N\bar{N})}_{\lambda_N\lambda_{\bar{N}},\lambda'_\gamma\lambda_\gamma}(t)=\frac{1}{(8\pi)}\,\frac{p_\pi}{\sqrt{t}}[T^{J(\gamma\gamma\to\pi\pi)}_{\Lambda_\gamma}(t)]\times[T^{J(\pi\pi\to N\bar{N})}_{\Lambda_N}(t)]^*. \tag{B8}$$

The partial wave amplitudes $T^{J(\pi\pi\to N\bar{N})}_{\Lambda_N}$ of Eq. (B7) are related to the amplitudes $f^J_\pm(t)$ of Frazer and Fulco [42] by the relations

$$T^{J(\pi\pi\to N\bar{N})}_{\Lambda_N=0}(t)=\frac{16\pi}{p_N}(p_Np_\pi)^J\cdot f^J_+(t),$$

$$T^{J(\pi\pi\to N\bar{N})}_{\Lambda_N=1}(t)=8\pi\frac{\sqrt{t}}{p_N}(p_Np_\pi)^J\cdot f^J_-(t), \tag{B9}$$

with p_N and p_π the c.m. momenta of nucleon and pion, respectively, ($p_N=\sqrt{t/4-M^2}$ and $p_\pi=\sqrt{t/4-m_\pi^2}$). For the reaction $\gamma\gamma\to\pi\pi$, we will use the partial wave amplitudes $F_{J\Lambda_\gamma}(t)$, which are related to those of Eq. (B6) by

$$T^{J(\gamma\gamma\to\pi\pi)}_{\Lambda_\gamma}(t)=\frac{2}{\sqrt{2J+1}}F_{J\Lambda_\gamma}(t). \tag{B10}$$

Denoting the Born partial wave amplitudes for $\gamma\gamma\to\pi^+\pi^-$ by $B_{J\Lambda_\gamma}(t)$, the lowest Born partial waves (s and d waves) are

$$B_{00}(t)=2e^2\frac{1-\beta^2}{2\beta}\ln\left(\frac{1+\beta}{1-\beta}\right),$$

$$B_{20}(t)=2e^2\frac{\sqrt{5}}{4}\frac{1-\beta^2}{\beta^2}\left\{\frac{3-\beta^2}{\beta}\ln\left(\frac{1+\beta}{1-\beta}\right)-6\right\},$$

$$B_{22}(t)=2e^2\frac{\sqrt{15}}{4\sqrt{2}}\left\{\frac{(1-\beta^2)^2}{\beta^3}\ln\left(\frac{1+\beta}{1-\beta}\right)+\frac{10}{3}-\frac{2}{\beta^2}\right\} \tag{B11}$$

with $\beta=p_\pi/(\sqrt{t}/2)$ the pion velocity.

Inserting the partial-wave expansion of Eq. (B4) into Eq. (B3), we can finally express the 2π t-channel contributions $\mathrm{Im}_t A_i(\nu=0,t)^{2\pi}$ by the partial wave amplitudes for the reactions $\gamma\gamma\to\pi\pi$ and $\pi\pi\to N\bar{N}$,

$$\begin{aligned}
\mathrm{Im}_t A_1(\nu=0,t)^{2\pi}\\
&=\frac{p_\pi}{\sqrt{t}}\frac{1}{tp_N^2}\sum_{J=0,2,4,\ldots}(p_\pi p_N)^J\sqrt{2J+1}F_{J\Lambda_\gamma=0}(t)f_+^{J*}(t)\\
&\quad\times\left[(-1)^{J/2}\frac{(J-1)!!}{J!!}\right],\\
\mathrm{Im}_t A_2(\nu=0,t)^{2\pi}&=0,\\
\mathrm{Im}_t A_3(\nu=0,t)^{2\pi}\\
&=\frac{p_\pi}{\sqrt{t}}\frac{M^2}{tp_N^4}\sum_{J=2,4,\ldots}(p_\pi p_N)^J\sqrt{2J+1}F_{J\Lambda_\gamma=2}(t)\\
&\quad\times\left[(-1)^{(J-2)/2}\sqrt{\frac{(J+1)J}{(J-1)(J+2)}}\frac{(J-1)!!}{J!!}\right]\\
&\quad\times\left\{f_+^{J*}(t)-f_-^{J*}(t)M\left[\frac{(J+2)(J-1)-2}{\sqrt{J(J+1)}}\right]\right\},\\
\mathrm{Im}_t A_4(\nu=0,t)^{2\pi}\\
&=-\frac{p_\pi}{\sqrt{t}}\frac{M^3}{tp_N^4}\sum_{J=4,\ldots}(p_\pi p_N)^J\sqrt{2J+1}F_{J\Lambda_\gamma=2}(t)f_-^{J*}(t)\\
&\quad\times\frac{(-1)^{(J-2)/2}2(J-2)(J+3)}{\sqrt{(J+2)(J-1)}}\frac{(J-1)!!}{J!!},\\
\mathrm{Im}_t A_5(\nu=0,t)^{2\pi}\\
&=-\frac{p_\pi}{\sqrt{t}}\frac{M}{tp_N^2}\sum_{J=2,4,\ldots}(p_\pi p_N)^J\sqrt{2J+1}F_{J\Lambda_\gamma=0}(t)f_-^{J*}(t)\\
&\quad\times\left[\frac{(-1)^{(J-2)/2}}{\sqrt{J(J+1)}}\frac{(J+1)!!}{(J-2)!!}\right],\\
\mathrm{Im}_t A_6(\nu=0,t)^{2\pi}\\
&=-\frac{p_\pi}{\sqrt{t}}\frac{M}{tp_N^2}\sum_{J=2,4,\ldots}(p_\pi p_N)^J\sqrt{2J+1}F_{J\Lambda_\gamma=2}(t)f_-^{J*}(t)\\
&\quad\times\left[\frac{(-1)^{(J-2)/2}[(J+2)(J-1)-2]}{\sqrt{(J+2)(J-1)}}\frac{(J-1)!!}{J!!}\right].
\end{aligned} \tag{B12}$$

We note that the s-wave ($J=0$) component of the 2π intermediate states contributes only to A_1. The amplitude A_2, corresponding to the exchange of pseudoscalar mesons (dominantly π^0) in the t channel, gets no contribution from 2π states, because the 2π system cannot couple to the nucleon through a pseudoscalar operator. Furthermore, it is found that only waves with $J\geqslant 4$ contribute to the amplitude A_4. In our calculations we saturate the t-channel dispersion integral with $s(J=0)$ and $d(J=2)$ waves, for which the expressions of Eq. (B12) reduce to those given in Eq. (40).

APPENDIX C: f_2-MESON CONTRIBUTION TO THE $\gamma\gamma\to\pi\pi$ PROCESS

A spin-2 particle is described in terms of a symmetric and traceless field tensor, with five independent components, satisfying the Klein-Gordon equation. Therefore, a state of spin-2 is characterized by a symmetric and traceless polarization tensor $\varepsilon^{\mu\nu}(p,\Lambda)$ $(\Lambda=-2,-1,0,1,2)$. For details, we refer to Ref. [43]. We will apply here this spin-2 formalism to describe the s-channel exchange of the f_2 meson in the process $\gamma\gamma\to\pi\pi$.

The coupling of the (isoscalar) $f_2(1270)$ meson (with momentum p and mass m_{f_2}) to a pion pair (with momenta p_π^μ, $p_\pi'^\mu$ and Cartesian isospin indices a,b) is described by the amplitude

$$\mathcal{M}(f_2\to\pi\pi)=\frac{g_{f_2\pi\pi}}{m_{f_2}}\delta_{ab}p_\pi'^\mu p_\pi^\nu\varepsilon_{\mu\nu}(p,\Lambda), \tag{C1}$$

where the coupling constant $g_{f_2\pi\pi}$ is determined from the $f_2\to\pi\pi$ decay width

$$\Gamma(f_2\to\pi\pi)=\frac{1}{40\pi}g_{f_2\pi\pi}^2\frac{(p_\pi)^5}{m_{f_2}^4}, \tag{C2}$$

where $p_\pi=\sqrt{m_{f_2}^2/4-m_\pi^2}$ is the pion three momentum in the f_2 rest frame. Using the partial width $\Gamma(f_2\to\pi\pi)=0.846\,\Gamma_0$ and the total f_2 width $\Gamma_0=185$ MeV [25], Eq. (C2) yields for the coupling: $g_{f_2\pi\pi}\simeq$ 23.64.

The Lorentz structure of the vertex $f_2\to\gamma\gamma$ is given by

$$\begin{aligned}
&\mathcal{M}(f_2\to\gamma\gamma)\\
&\quad=-i2e^2\frac{g_{f_2\gamma\gamma}}{m_{f_2}}\mathcal{F}^{\mu\delta}(q,\lambda_\gamma)\mathcal{F}_\delta^\nu(q',\lambda_\gamma')\varepsilon_{\mu\nu}(p,\Lambda),
\end{aligned} \tag{C3}$$

where $\mathcal{F}^{\alpha\beta}$ is the electromagnetic field tensor. Using the vertex of Eq. (C3), the $f_2\to\gamma\gamma$ decay width is calculated as

$$\Gamma(f_2\to\gamma\gamma)=\frac{e^4}{80\pi}g_{f_2\gamma\gamma}^2m_{f_2}. \tag{C4}$$

Using the partial width $\Gamma(f_2\to\gamma\gamma)=1.32\times10^{-5}\Gamma_0$ [25], Eq. (C4) determines the value of the coupling constant: $g_{f_2\gamma\gamma}\simeq$ 0.239.

Using these couplings and vertices, we can now calculate the invariant amplitude for the process $\gamma\gamma\to f_2\to\pi\pi$:

$$\mathcal{M}(\gamma\gamma\to f_2\to\pi\pi)=-i2e^2\frac{g_{f_2\gamma\gamma}}{m_{f_2}}\mathcal{F}^{\mu\delta}(q,\lambda_\gamma)\times\mathcal{F}^{\nu}_{\delta}(q',\lambda'_\gamma)\Delta_{\mu\nu\alpha\beta}(p,\Lambda)\frac{g_{f_2\pi\pi}}{m_{f_2}}p^{\alpha}_{\pi}p'^{\beta}_{\pi},\tag{C5}$$

where $\Delta_{\mu\nu\alpha\beta}(p,\Lambda)$ represents the spin-2 propagator (see Ref. [43]). To determine the $\gamma\gamma\to\pi\pi$ helicity amplitudes F_{Λ_γ} defined in Eq. (28), we shall evaluate Eq. (C5) in the c.m. system. For the case of equal photon helicities ($\Lambda_\gamma=0$) the f_2 does not contribute, i.e., $F^{(f_2)}_{\Lambda_\gamma=0}=0$. For the case of opposite photon helicities ($\Lambda_\gamma=2$) we find after some algebra

$$F^{(f_2)}_{\Lambda_\gamma=2}=-\frac{e^2}{8}\frac{g_{f_2\gamma\gamma}g_{f_2\pi\pi}}{m^2_{f_2}}\frac{t^2\beta^2}{t-m^2_{f_2}+im_{f_2}\Gamma_0}\sin^2\theta_{\pi\pi},\tag{C6}$$

where $\theta_{\pi\pi}$ is the pion c.m. angle and β the pion velocity as in Eq. (28). It is immediately seen from Eq. (C6) that the f_2 meson contribution to the d wave is given by

$$F^{(f_2)}_{J=2\Lambda_\gamma=2}(t)=-\sqrt{\frac{2}{15}}\frac{e^2}{4}\frac{g_{f_2\gamma\gamma}g_{f_2\pi\pi}}{m^2_{f_2}}\frac{t^2\beta^2}{t-m^2_{f_2}+im_{f_2}\Gamma_0}.\tag{C7}$$

[1] F. J. Federspiel, R. A. Eisenstein, M. A. Lucas, B. E. MacGibbon, K. Mellendorf, A. M. Nathan, A. O'Neill, and D. P. Wells, Phys. Rev. Lett. **67**, 1511 (1991).
[2] A. Zieger, R. Van de Vyver, D. Christmann, A. De Graeve, C. Van den Abeele, and B. Ziegler, Phys. Lett. B **278**, 34 (1992).
[3] E. L. Hallin *et al.*, Phys. Rev. C **48**, 1497 (1993).
[4] B. E. MacGibbon, G. Garino, M. A. Lucas, A. M. Nathan, G. Feldman, and B. Dolbilkin, Phys. Rev. C **52**, 2097 (1995).
[5] A. L'vov, V. A. Petrun'kin, and M. Schumacher, Phys. Rev. C **55**, 359 (1997).
[6] C. Molinari *et al.*, Phys. Lett. B **371**, 181 (1996).
[7] J. Peise *et al.*, Phys. Lett. B **384**, 37 (1996).
[8] J. Tonnison, A. M. Sandorfi, S. Hoblit, and A. M. Nathan, Phys. Rev. Lett. **80**, 4382 (1998).
[9] V. Bernard, N. Kaiser, and U.-G. Meissner, Phys. Rev. Lett. **67**, 1515 (1991).
[10] V. Bernard, N. Kaiser, A. Schmidt, and U.-G. Meissner, Phys. Lett. B **319**, 269 (1993); Z. Phys. A **348**, 317 (1994).
[11] T. R. Hemmert, B. R. Holstein, and J. Kambor, Phys. Lett. B **395**, 89 (1997).
[12] T. R. Hemmert, B. R. Holstein, and J. Kambor, Phys. Rev. D **55**, 5598 (1997).
[13] T. R. Hemmert, B. R. Holstein, J. Kambor, and G. Knöchlein, Phys. Rev. D **57**, 5746 (1998).
[14] V. Bernard, N. Kaiser, J. Kambor, and U.-G. Meissner, Nucl. Phys. **B388**, 315 (1992); Int. J. Mod. Phys. E **4**, 193 (1995).
[15] D. Drechsel, G. Krein, and O. Hanstein, Phys. Lett. B **420**, 248 (1998).
[16] A. I. L'vov and A. M. Nathan, Phys. Rev. C **59**, 1064 (1999).
[17] A. M. Baldin, Nucl. Phys. **18**, 310 (1960); L. I. Lapidus, Zh. Éksp. Teor. Fiz. **43**, 1358 (1962) [Sov. Phys. JETP **16**, 964 (1963)].
[18] M. Damashek and F. J. Gilman, Phys. Rev. D **1**, 1319 (1970).
[19] D. Babusci, G Giordano, and G. Matone, Phys. Rev. C **57**, 291 (1998).
[20] A. M. Sandorfi, C. S. Whisnant, and M. Khandaker, Phys. Rev. D **50**, R6681 (1994).
[21] J. Ahrens *et al.*, MAMI proposal 12/2-93 (1993); H. J. Arends, *Proceedings of the 8th International Conference on the Structure of Baryons* (Baryons 98), Bonn, Germany, 1998, edited by D. W. Menze and B. Metsch (World Scientific, Singapore, 1999).
[22] D. Babusci, G. Giordano, A. I. L'vov, G. Matone, and A. M. Nathan, Phys. Rev. C **58**, 1013 (1998).
[23] D. M. Akhmedov and L. V. Fil'kov, Yad. Fiz. **33**, 1083 (1981) [Sov. J. Nucl. Phys. **33**, 573 (1981)].
[24] B. R. Holstein and A. M. Nathan, Phys. Rev. D **49**, 6101 (1994).
[25] Particle Data Group, C. Caso *et al.*, Eur. Phys. J. C **3**, 1 (1988).
[26] R. A. Arndt, R. L. Workman, I. I. Strakovsky, and M. M. Pavan, nucl-th/9807087.
[27] S. Ragusa, Phys. Rev. D **47**, 3757 (1993); **49**, 3157 (1994).
[28] O. Hanstein, D. Drechsel, and L. Tiator, Nucl. Phys. **A632**, 561 (1998).
[29] R. A. Arndt, I. I. Strakovsky, and R. L. Workman, Phys. Rev. C **53**, 430 (1996).
[30] M. Benmerrouche and N. C. Mukhopadhyay, Phys. Rev. D **46**, 101 (1992).
[31] D. Drechsel, S. S. Kamalov, G. Krein, and L. Tiator, Phys. Rev. D **59**, 094021 (1999).
[32] R. A. Arndt, R. L. Workman, Z. Li, and L. D. Roper, Phys. Rev. C **42**, 1853 (1990); **42**, 1864 (1990).
[33] D. Drechsel and G. Krein, Phys. Rev. D **58**, 116009 (1998).
[34] D. Morgan and M. R. Pennington, Z. Phys. C **37**, 431 (1988).
[35] M. R. Pennington, in *The Second DaΦne Physics Handbook*, edited by L. Maiani, G. Pancheri, and N. Paver (INFN, Frascati, 1995).
[36] C. D. Froggatt and J. L. Petersen, Nucl. Phys. **B129**, 89 (1977).
[37] G. Höhler, *Pion-Nucleon Scattering*, Landolt-Börnstein, Vol. I/9b2, edited by H. Schopper (Springer, Berlin, 1983).
[38] G. Blanpied *et al.*, Phys. Rev. Lett. **79**, 4337 (1997); **76**, 1023 (1996).
[39] A2 Collaboration at MAMI: J. Ahrens (private communication); V. Olmos de Léon (private communication); F. Wissmann (private communication).
[40] R. E. Prange, Phys. Rev. **110**, 240 (1958).
[41] W. A. Bardeen and W. K. Tung, Phys. Rev. **173**, 1423 (1968).
[42] W. R. Frazer and J. R. Fulco, Phys. Rev. **117**, 1603 (1960).
[43] D. Spehler and S. F. Novaes, Phys. Rev. D **44**, 3990 (1991).